NATIONAL & KAPODISTRIAN
UNIVERSITY OF ATHENS

MASTER THESIS

A twin numerical model experiment for assessing the impact of the Black Sea Water inflow on the Aegean dynamics and biogeochemistry

Author:
Evangelia Boza
(7114122100007)

Supervisor:
Assoc. Prof. Sarantis Sofianos

MSc in Oceanography and Management of the Marine Environment
Specialization: Physical Oceanography

Athens, Greece
September 2023

The present thesis was conducted at the Ocean Physics and Modelling Group of the Physics Department of NKUA as part of the Inter-Institutional Postgraduate program NKUA-HCMR in the Oceanography and Management of the Marine Environment.

***Dissertation Committee*:**

Assoc. Prof. **Sarantis Sofianos** (Supervisor)

Department of Physics

NKUA

Dr. **Vassilios Vervatis**

Department of Physics

NKUA

Assist. Prof. **Dionysios Raitsos**

Department of Biology

NKUA

Athens, Greece
September 2023

Abstract

Black Sea Water (BSW) inflow into the Aegean Sea is of great importance for shaping the hydrography and circulation patterns not only in the Aegean, but also across the entire Eastern Mediterranean Sea. In addition to its influence on the region's physical processes, the exchange water fluxes through the Dardanelles Strait can also exert a significant effect on its biogeochemical characteristics. In this study, we employ a twin numerical model experiment to investigate the impacts of the BSW inflow into the Aegean Sea, from both physical and biogeochemical perspectives. To accomplish this, we utilize a coupled ocean–biogeochemical configuration of the ocean model NEMO (Nucleus for European Modelling of the Ocean), covering the Mediterranean and Black Seas at 1/12° resolution. The twin experiment comprises two simulations: one representing the actual conditions of the study region, with BSW flowing into the North Aegean, and the other depicting a hypothetical scenario in which the Dardanelles Strait is sealed off, resulting in a complete absence of BSW inflow into the study area. The experiments were carried out for a 5-year period, from 2008 to 2012. In the results, we focus on the last year (2012), showcasing the variations of several upper-ocean and vertical thermohaline and biogeochemical properties, for each experiment, as well as for their difference. In summary, we find that BSW has a pronounced impact on various properties and processes of the North Aegean Sea. Some of the most important outcomes are the significant reduction in Sea Surface Salinity levels, the intensification of the mesoscale eddies of the region and, potentially, the hindering of deep water formation processes. Additionally, the presence of BSW leads to higher levels of chlorophyll and nutrients in the North Aegean, while oxygen concentrations rise on the surface and decrease in deeper layers of the study area.

Keywords: Ocean Modelling; twin experiment; NEMO; Aegean; Black Sea Water

Περίληψη

Η εισροή υδάτων από την Μαύρη Θάλασσα στο Αιγαίο αποτελεί καθοριστικό παράγοντα στην διαμόρφωση των υδρολογικών χαρακτηριστικών και των κυκλοφοριακών προτύπων όχι μόνο για το Αιγαίο, αλλά και για την ευρύτερη περιοχή της Ανατολικής Μεσογείου. Σε συνδυασμό με την επίδρασή τους στις φυσικές διεργασίες της περιοχής, οι ανταλλαγές των ροών υδάτων μέσω του στενού των Δαρδανελίων μπορούν να ασκήσουν σημαντική επίδραση και στα βιογεωχημικά χαρακτηριστικά της. Σε αυτή την μελέτη, χρησιμοποιούμε ένα δίδυμο αριθμητικό πείραμα για να εξετάσουμε τις επιπτώσεις που προκύπτουν από την εισροή των υδάτων της Μαύρης Θάλασσας στο Αιγαίο, σε ό,τι αφορά τις φυσικές και βιογεωχημικές διεργασίες. Προκειμένου να το επιτύχουμε αυτό, χρησιμοποιούμε ένα συζευγμένο φυσικό-βιογεωχημικό μοντέλο για την Μεσόγειο και την Μαύρη Θάλασσα με οριζόντια ανάλυση 1/12º, βασισμένο στην πλατφόρμα ωκεανογραφικών μοντέλων NEMO. Το δίδυμο πείραμα περιλαμβάνει δύο προσομοιώσεις: το πρώτο πείραμα προσομοιώνει τις πραγματικές συνθήκες που επικρατούν στην περιοχή μελέτης, όπου τα νερά της Μαύρης Θάλασσας εισέρχονται στο Αιγαίο, ενώ το δεύτερο προσομοιώνει ένα υποθετικό σενάριο, στο οποίο το στενό των Δαρδανελίων είναι φραγμένο, με αποτέλεσμα την μηδενική εισροή υδάτων από την Μαύρη Θάλασσα προς το Αιγαίο. Τα πειράματα διεξήχθησαν για μια πενταετία, από το 2008 μέχρι και το 2012. Στα αποτελέσματα εστιάζουμε στην τελευταία χρονιά των προσομοιώσεων (2012), παρουσιάζοντας τις μεταβολές διαφόρων επιφανειακών και κατά βάθος θερμοαλατικών και βιογεωχημικών μεταβλητών, για κάθε πείραμα, αλλά και για την διαφορά τους. Συνοπτικά, διαπιστώνουμε ότι η εισροή των υδάτων της Μαύρης Θάλασσας έχει έντονη επίδραση στα χαρακτηριστικά και τις διεργασίες του Βόρειου Αιγαίου. Ορισμένα βασικά συμπεράσματα είναι ότι οι τιμές της επιφανειακής αλατότητας μειώνονται σημαντικά, οι κυκλωνικοί και αντικυκλωνικοί σχηματισμοί της περιοχής ενισχύονται, ενώ οι διαδικασίες δημιουργίας βαθιών νερών φαίνεται να εμποδίζονται. Επιπλεόν, η εισροή υδάτων της Μαύρης Θάλασσας οδηγεί σε υψηλότερα επίπεδα χλωροφύλλης και θρεπτικών ουσιών στο Βόρειο Αιγαίο, ενώ παράλληλα οι συγκεντρώσεις οξυγόνου αυξάνονται στην επιφάνεια και μειώνονται στα βαθύτερα στρώματα της εξεταζόμενης περιοχής.

Contents

Chapter 1

Introduction

1.1 Background and motivation

The Mediterranean Sea is a culturally and economically significant region, hosting numerous countries and supporting various industries such as tourism, fishing, and trade. Its unique geographical characteristics and historical importance have shaped the civilizations around its shores for thousands of years. Furthermore, it can be described as a partially enclosed body of water, serving as a connection between the Atlantic Ocean via the Strait of Gibraltar and the Black Sea through the Bosporus Strait. It also exhibits physical processes that closely resemble or mirror those observed in the global oceanic circulation. The Aegean Sea constitutes a part of the Eastern Mediterranean Sea (EMED), holding significant importance in shaping the dynamics of the entire Mediterranean region. The northern part of the Aegean is characterized as one of the most productive areas of the EMED, owing to the Black Sea Water (BSW) discharge in the region (Ignatiades et al., 2002; Siokou-Frangou et al., 2009; Kalaroni et al., 2020). In addition to its noteworthy impact on the biogeochemistry of the Aegean, BSW influences the physical processes of the area, as well (Tzali et al., 2010; Androulidakis et al., 2012b; Mavropoulou et al., 2016).

The purpose of the present thesis is to investigate the impact of the BSW inflow on the dynamics and biogeochemistry of the Aegean Sea, using a twin numerical model experiment. The objective is to identify how the BSW affects the temporal and spatial distribution of various thermohaline and biogeochemical characteristics, Additionally, we seek to comprehend the alternations in the physical processes of the North Aegean Sea resulting from the absence of BSW inflow. In order to study these impacts, two experiments were performed over a 5-year period using a state-of -the art coupled physical-biogeochemical model. The first experiment represents

the actual environmental conditions during the examined period. The second experiment simulates the imaginary scenario, where there is a total absence of BSW inflow into the Aegean Sea. Due to the limited simulation period that we examine, the study focuses on the North Aegean region, which is the first receptor of BSW, and thus, undergoes the initial and most significant alterations within the entire Aegean Sea.

The thesis is organized as follows: In Chapter 2, we describe the model configuration and outline the experimental design adopted in the study. Moving on to Chapter 3, we analyze the model results on a temporal and spatial scale for both experiments, focusing on both upper-ocean and vertical properties. Lastly, in Chapter 4 a concise summary and conclusion of the results is presented.

1.2 The study area

1.2.1 Geographical location and geomorphology

The Eastern Mediterranean Sea (EMED) encompasses various regions situated to the east of the Sicily Strait. This includes the Levantine basin, the Adriatic Sea, the Aegean Sea, and the Ionian Sea, which is recognized as the deepest basin within the Eastern Mediterranean. This study primarily focuses on the Aegean Sea, a region known for its intricate hydrology, water masses, circulation patterns, and biogeochemical processes (Lykousis et al., 2002). The Aegean Sea is geographically enclosed by the Turkish coastline to the east, the Greek mainland to the north and west, and the island of Crete to the south. The region's bottom topography displays a distinctive pattern of plateaus and deep troughs. One notable feature is the Cyclades plateau, which acts as a separator between the North and South Aegean basins. This plateau facilitates water exchange at depths above 400 m (Siokou-Frangou et al., 2002). At depths below 400 m, the deep basins of the North Aegean contain locally sourced dense water (Zervakis et al., 2000), while the deep basin of the South Aegean is filled with Cretan Deep Water (Theocharis et al., 1999). The North Aegean Sea, in particular, has numerous small and large islands, along with

gulfs and deep depressions like the notable North Aegean Trough (**Figure 1**). The North Aegean Trough stands out as a prominent feature of the region, comprising multiple sub-basins including the North Sporades Basin, which reaches a maximum depth of 1,000 m, as well as the Limnos and Saros Basins. Additionally, the presence of widespread plateaus like the Thermaikos and Samothraki plateau, with depths of less than 200 m, significantly influences the hydrological characteristics of the area.

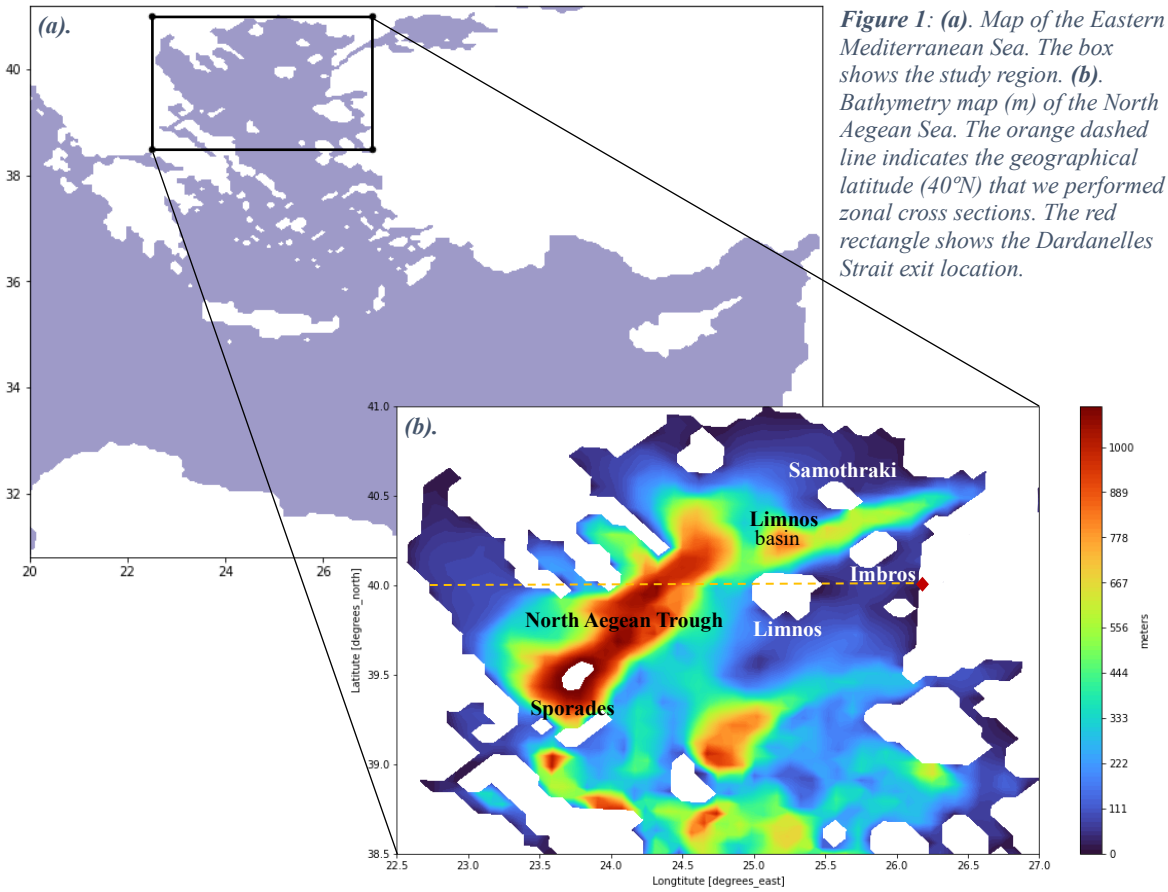

***Figure 1**: **(a)**. Map of the Eastern Mediterranean Sea. The box shows the study region. **(b)**. Bathymetry map (m) of the North Aegean Sea. The orange dashed line indicates the geographical latitude (40°N) that we performed zonal cross sections. The red rectangle shows the Dardanelles Strait exit location.*

An additional noteworthy aspect regarding the Aegean Sea is that it constitutes a link between the Mediterranean Sea and the Black Sea, acting as the initial recipient of water from the Black Sea via the Turkish Strait System (TSS). The TSS encompasses the Dardanelles Straits (DS), the Marmara Sea, and the Bosporus Strait.

1.2.2 Thermohaline circulation

The water exchange within the TSS exhibits a distinctive two-layer structure. The upper layer consists of brackish water known as BSW inflow, which moves towards the North Aegean Sea. In contrast, the lower layer, referred to as the outflow, comprises high-salinity water that flows roughly northeastward into the Marmara Sea. This two-layer exchange flow is primarily driven by differences in density and sea elevation between the basins (Ünlüata et al., 1990; Jarosz et al., 2012).

The BSW, initially with a salinity of around 17.8 psu, enters the Sea of Marmara as a surface layer with a salinity of approximately 19.4 psu. While passing through the Sea of Marmara, its salinity further increases by about 6 psu. Upon exiting the Dardanelles, the salinity reaches 29.6 psu after an additional increase of approximately 4 psu. In contrast, the Aegean water enters the Dardanelles with a salinity of 38.9 psu, and it undergoes minimal changes in its salt content while traversing the strait. However, within the Marmara basin, a reduction in the salinity of this water is observed, with a decrease of nearly 2 psu. Following an additional reduction of approximately 2 psu during its passage through the Bosporus, the Mediterranean waters flow into the Black Sea with a salinity level of nearly 35 psu (Ünlüata et al., 1990). Moreover, the hydrodynamic and physical characteristics of the North Aegean Sea, particularly in the upper layers, are significantly influenced by the prevailing meteorological conditions of the region. These conditions play a crucial role in shaping the dominant patterns and properties of the water flow within the area.

As noted by Tzali et al. (2010), the spread of BSW in the North Aegean and its impact on the circulation are directly linked to the volume of inflow through the Dardanelles Strait. Several studies have estimated the exchange rate in the Dardanelles using either in situ observations or parametrizations. Nevertheless, significant uncertainties remain regarding the fluctuation of inflow/outflow rates over various time scales, primarily due to the limited availability of long-term observational data from the Dardanelles Strait. Proposed volume fluxes exhibit varying seasonal patterns and amplitudes. While there are differences in the annual exchange rates reported by different studies, there is a consensus that the net mean

annual inflow rate into the North Aegean Sea is approximately 9.51×10^{-3} Sv (Mavropoulou et al., 2016).

The flows in the region follow a seasonal pattern, which is closely linked to the seasonal cycle of riverine freshwater inflow into the Black Sea (Ünlüata et al., 1990). The peak river discharge rates typically occur in May, while the signal reaches the TSS approximately two months later, as observed by Oğuz and Sur (1989). Consequently, it can be concluded that the maximum influx BSW into the Aegean occurs during late summer (**Figure 2b**), coinciding with the lowest salinity values of BSW in the northeastern part of the basin (Beşiktepe et al., 1994; Zodiatis, 1994; Zervakis et al., 2000).

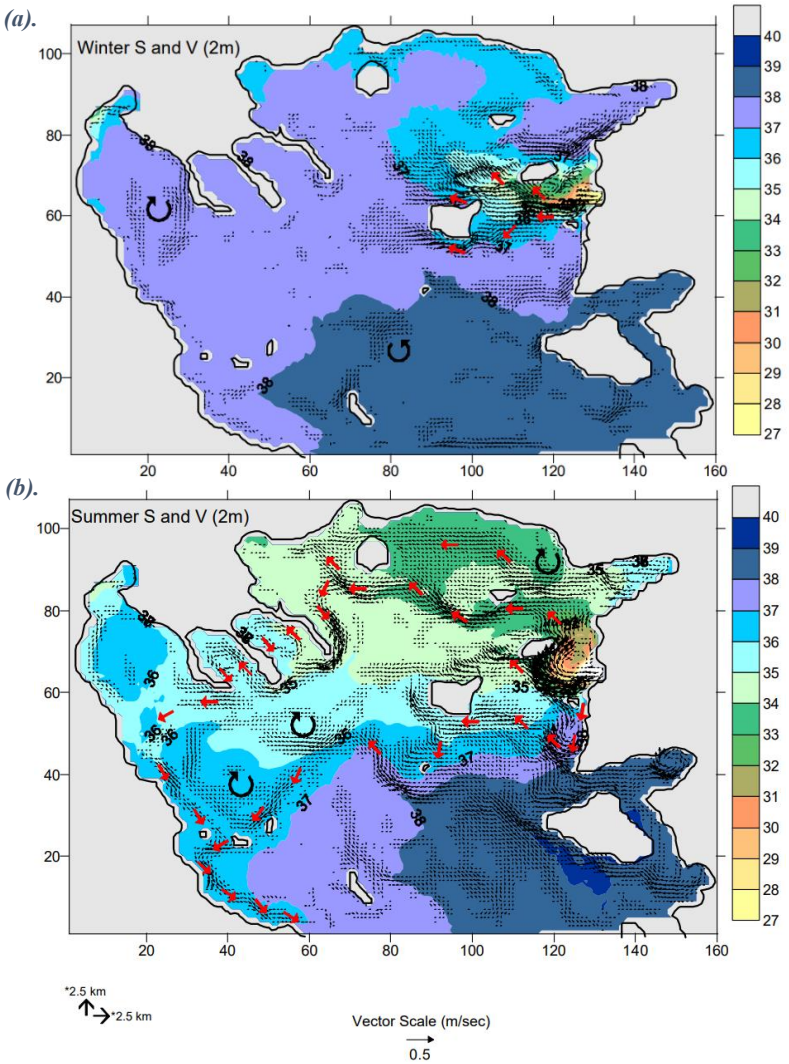

***Figure 2**: Model simulated salinity and current velocity at 2 meters depth during the **(a)** winter and **(b)** summer season (with a minimum velocity of 5 cm/s). The red arrows indicate the prevailing routes taken by waters originating from the BSW, while the curved black arrows highlight notable eddies in the area (Kourafalou and Barbopoulos, 2003).*

One of the prominent characteristics of the North Aegean Sea is the formation of a strong thermohaline front. This front emerges as a result of the surface inflow of brackish BSW interacting with the surrounding saltier and warmer waters originating from the Levantine region (Vlasenko et al., 1996). According to Zodiatis (1994), the front's location near the island of Limnos experiences constant variations, resulting in the formation of powerful currents that play a significant role in shaping the circulation pattern within the North Aegean region (**Figure 2**). Nonetheless, the most prominent and dynamic characteristics in the region are the mesoscale cyclonic and anticyclonic eddies (Sofianos et al., 2005).

Furthermore, the inflow of BSW creates a plume that extends westward, aligning with the overall cyclonic circulation pattern observed in the basin (Kourafalou and Barbopoulos, 2003; Lykousis et al., 2002). Subsequently, the inflow of the BSW departs from the North Aegean, tracing the path of the Evoia current along the western shores of the Aegean Sea (**Figure 2b**). East of Lemnos Island, a division in the current is frequently observed, with the northern branch contributing to the formation of a strong anticyclone around the island of Samothraki (Zervakis and Georgopoulos, 2002).

As reported by SoHelME in 2005, within the Mediterranean Sea, the Aegean Sea stands out as the area experiencing the highest rates of heat, freshwater, and buoyancy loss. In specific, the lightweight, brackish waters originating from the Black Sea via TSS play a crucial role in regulating the process of deep water formation across the basin, owing to two factors. Firstly, the presence of the BSW forms a thin surface layer, characterized by lower temperatures compared to the underlying waters, sourced from the Aegean/Levantine region. This particular condition effectively minimizes heat losses to the atmosphere during the winter months (Tragou et al., 2021). Secondly, the lateral buoyancy inflow through the Dardanelles Strait leads to a reduction in surface density and an increase in stratification, thereby impending the formation of highly dense waters. Gertman et al. (2006) yielded the conclusion that the BSW plays a crucial role in regulating the intensity of deep water formation in the region. Furthermore, they found that changes in the BSW have had a significant impact on the occurrence of the Eastern Mediterranean Transient (EMT) in the early 1990s. EMT has been extensively studied by researchers such as Roether et al. (1996), Zervakis et al. (2000), and Theocharis et al. (1999).

1.3 Biogeochemistry of the Mediterranean and Aegean Sea

The Mediterranean Sea stands out as one of the most oligotrophic seas, which is primarily attributed to its extremely low phosphate concentrations (Krom et al., 1991; Thingstad et al., 2005a). As a result, it fits the classification of a Low Nutrient - Low-Chlorophyll system (LNLC) (Durrieu de Madron et al., 2011). This oligotrophic characteristic is extensively documented and is known to exhibit a well-defined gradient, increasing from the western to the eastern parts of the basin (Turley et al., 2000; D'Ortenzio and Ribera d'Alcala, 2009). Throughout the entire year, the uppermost layers of the Mediterranean Sea show notably low levels of chlorophyll-a concentration and primary production. This pattern is consistent except for a brief period during late winter mixing events. However, a significant exception occurs at the upper edge of the nutricline, where a deep chlorophyll maximum (DCM) is observed. This DCM sustains the levels of chlorophyll-a and primary production. Notably, the depth at which this DCM occurs varies with location, becoming deeper as one moves eastward (Siokou-Frangou et al., 2010).

The decline in subsurface concentrations of dissolved inorganic nitrogen (N) and phosphorus (P) from west to east significantly shapes various aspects of the ecosystem, such as the abundance of photosynthetic biomass, concentrations of chlorophyll-a (Chl-a), and primary productivity (Krom et al., 2010). In the eastern basin, the dynamics of phytoplankton mirror those found in subtropical waters, characterized by minimal variations in Chl-a levels throughout the year. Notably, the Aegean, Levantine, and Ionian basins are categorized as regions where significant blooms are not common. Instead, they exhibit a bimodal pattern, with lower biomass during late spring and summer, and a rise in biomass leading up to the maximum levels in late fall and winter (D'Ortenzio and Ribera d'Alcala, 2009; Lavigne et al. 2015; Barbieux et al., 2018).

In the research conducted by Kalaroni et al. (2020), an investigation was undertaken to establish a preliminary biogeographic division of the Mediterranean basin. This division aimed to effectively verify the intricate spatial-temporal results generated by the ecosystem model through comparison with observational data. In terms of productivity, the most productive eco-region includes zones that receive substantial lateral nutrient inputs. These include the Alboran Sea influenced by the inflow of

Atlantic Water, significant river systems, and areas where BSW is discharged. The second most productive eco-region encompasses the entire western basin, including areas impacted by cyclonic water circulation that typically trigger greater vertical mixing. Examples of this are the Gulf of Lion and the North-West Mediterranean Sea. This category also involves the North Aegean and North Adriatic Seas, which benefit from substantial nutrient loads from sizable river systems. In contrast, the South Adriatic, Ionian, South Aegean Seas, and the South-East Mediterranean Sea represent the most oligotrophic eco-regions in the Mediterranean basin. These areas are characterized by low levels of Chl-a, phosphate, and nitrate, as well as relatively elevated temperatures.

As mentioned previously, the productivity levels in the North Aegean region are notably impacted by the BSW inflow, an influence that displays significant year-to-year variation (Petihakis et al., 2014). The TSS regulates the transfer of various substances such as chemicals, biological matter, and fish between the Black Sea and the Mediterranean Sea. When water flows through the TSS and enters the northern Aegean Sea, it affects the recycling of nutrients, productivity levels, and the feeding patterns of both local and migrating species. While there is extensive documentation on the hydrological aspects of the TSS (Özsoy et al., 2002), there is a scarcity of biological data available. Furthermore, the inflow of BSW into the North Aegean brings with it elevated levels of dissolved organic carbon and nitrogen (Polat and Tugrul 1996; Lykousis et al., 2002). Additionally, this inflow has a profound impact on plankton production in the region, resulting exceptionally high levels for both autotrophs and heterotrophs (Ignatiades et al., 2002; Siokou-Frangou et al., 2002).

The MTP-II-MATER project (1996-1999) was a groundbreaking effort to understand the complex interactions within the Aegean Sea ecosystem. Various factors were identified as crucial for the Aegean's biogeochemical dynamics, carbon cycle, and energy transfer. These factors included meso-scale circulation, deep water masses, river inputs, BSW inflow, changes in productivity, seafloor topography, and potentially dust inputs. Additionally, significant variations were observed between the Northern and Southern Aegean regions, regarding the nutrient levels, POC, Chl-a concentration, phytoplankton and mesozooplankton abundance, primary production, and bacteria production. Despite these differences, the entire Aegean Sea was found to be generally oligotrophic. Concerning the influence of BSW, it was found that while the Northern Aegean showed limited influence from BSW in terms

of certain parameters, it did exhibit noticeable impacts in terms of dissolved components like dissolved organic carbon (DOC) and trace elements like manganese (Mn). Moreover, the deep basins in the North Aegean were identified as areas with high levels of organic matter accumulation and significant benthic abundance and biodiversity. Differences in biogeochemical and benthic processes were observed from north to south, influenced by various factors, including seasonal changes, inputs from surrounding areas, and the presence of mesoscale eddies, which cause further east-to-west gradients within the Southern Aegean Sea (Lykousis et al., 2002).

Chapter 2

Methodology and experimental design

This thesis utilizes the Nucleus for European Modelling of the Ocean – NEMO (Madec et al., 2023), which is a comprehensive framework consisting of various engines designed to investigate the ocean and its intricate connections with other components of the Earth's climate system across extensive temporal and spatial scales. The primary engines within this framework include OPA, responsible for studying ocean dynamics and thermodynamics, LIM, which examines sea-ice dynamics and thermodynamics, and TOP, specifically dedicated to biogeochemistry.

2.1 Physical model NEMO

We are employing a model that tackles the three-dimensional primitive equations, incorporating a nonlinear equation of state. This equation connects the fluid velocity with two active tracers, temperature and salinity, within an Arakawa C-grid framework. The model assumes an incompressible and hydrostatic fluid, considering a spherical Earth with a thin shell approximation. Additionally, it incorporates the Boussinesq approximation and the hypothesis of turbulence closure. To facilitate calculations, we employ an orthogonal set of unit vectors (i, j, k) aligned with the Earth's reference frame. Our focus is on solving the following equations:

- *Momentum Balance:*

$$\frac{\partial \mathbf{U}_h}{\partial t} = [(\nabla \times \mathbf{U}) \times \mathbf{U}) + \frac{1}{2} \nabla (\mathbf{U}^2)]_h - f\mathbf{k} \times \mathbf{U}_h - \frac{1}{\rho_o} \nabla_h p + \mathbf{D}^{\mathbf{U}} + \mathbf{F}^{\mathbf{U}}$$

- *Hydrostatic equilibrium:*

$$\frac{\partial p}{\partial z} = -\rho g$$

- *Incompressibility equation:*

$$\nabla \cdot \mathbf{U} = 0$$

- *Heat conservation equation:*

$$\frac{\partial T}{\partial t} = -\nabla \cdot (T\mathbf{U}) + D^T + F^T$$

- *Salt conservation equation:*

$$\frac{\partial S}{\partial t} = -\nabla \cdot (S\mathbf{U}) + D^S + F^S$$

- *Equation of state:*

$$\rho = \rho(T, S, p)$$

In the equations we are working with, we express the vector velocity as the sum of the horizontal component $\boldsymbol{U}k$ and the vertical component $w\boldsymbol{k}$, denoted as $\boldsymbol{U}$. The variables T and S represent the potential temperature and salinity, respectively. The in-situ density is represented by ρ, with ρ_0 being a reference density. The pressure is denoted as p, and the term f = 2Ωk represents the Coriolis acceleration, where Ω represents Earth's angular velocity vector. The gravitational acceleration is represented by g. Parameterizations of small-scale physics for momentum, temperature, and salinity are captured by D^U, D^T, and D^S, respectively. Additionally, the equations include surface forcing terms F^U, F^T, and F^S, which account for external influences on momentum, temperature, and salinity at the fluid's surface.

The ocean mesh, which determines the positions of scalar and vector points, is established through a transformation that maps the geographical coordinate system (λ, ϕ, z) to orthogonal curvilinear coordinates (i, j, k). In this transformation, the latitude coordinate is represented by λ(i, j), while the longitude coordinate is denoted by φ(i, j). This relationship allows us to map the geographical coordinates onto the curvilinear coordinate system, defining the spatial arrangement of points within the ocean mesh.

2.2 Biogeochemical model PISCES

PISCES v2, a biogeochemical model developed by Aumont et al. (2015), is an integral component of the NEMO modeling platform. Its primary purpose is to simulate and analyze ocean productivity and biogeochemical cycles. The model encompasses 24 prognostic variables, enabling a comprehensive analysis of these processes. Regarding phytoplankton growth, there exist five key nutrients that impose limitations: nitrate and ammonium, phosphate, silicate, and iron. The interrelationship between phosphate, nitrate and ammonium is established through a consistent Redfield ratio C/N/P (122/16/1; Takahashi et al., 2014). This ratio governs the distribution of these elements across all organic components within the PISCES model. Within the model, there are two distinct categories for phytoplankton based on their size: nanophytoplankton and diatoms. For these categories, the prognostic variables include the total biomass in terms of carbon, iron, chlorophyll, and silicon (the latter only for diatoms). Consequently, the ratios of Fe/C, Chl/C, and Si/C are not fixed but rather variable and determined by the model through prognostic predictions. Moreover, the model incorporates two size classes for zooplankton: microzooplankton and mesozooplankton. These classes maintain constant ratios within the model. Therefore, the total biomass in terms of carbon serves as the sole prognostic variable for zooplankton.

It's important to note that the model does not explicitly simulate the bacterial pool. PISCES encompasses three distinct non-living pools to represent organic carbon: small particulate organic carbon, big particulate organic carbon, and semi-labile dissolved organic carbon. The composition of dissolved and particulate matter in terms of carbon, nitrogen, and phosphorus follows the Redfield stoichiometry. However, the iron content within the particles is computed prognostically by the model. Additionally, the model includes the simulation of calcium carbonate (calcite) and biogenic silicate particles. Furthermore, the model takes into account the carbonate system, encompassing dissolved inorganic carbon and total alkalinity, as well as dissolved oxygen and pH. The biogeochemical parameters employed in the model adhere to the standard parameters of PISCESv2. For a comprehensive understanding of the model, the detailed description is provided by Aumont et al. (2015).

2.3 Model Configuration

The model domain encompasses the Mediterranean and Black Seas, which are explicitly interconnected through the Marmara Sea via the (open) Dardanelles and Bosporus strait, and it spans a geographic range between 30ºN - 50.39ºN and 9.07ºW - 42.62ºE. The NEMO model configuration employed in this study was initiated in the context of work of Karagiorgos et al. (2023) and closely resembles the setup utilized by Varlas et al. (2020). To establish initial and open boundary conditions, daily ocean reanalysis fields from the GLORYS12 product of the Copernicus Marine Environment and Monitoring Service (CMEMS) were utilized. These reanalysis fields corresponded to the same 1/12° horizontal resolution as the ocean model configuration. It is important to note that there was no local data assimilation within the model domain during the forecast period. The grid utilized in this study follows the Arakawa C-type grid, featuring a spatial horizontal resolution of 1/12° × 1/12°. It encompasses a total of 609 gridboxes in the East-West direction and 320 gridboxes in the North-South direction. For the vertical analysis, a non-uniform thickness approach was employed, dividing the analysis into 50 levels. The western boundary of the model was designed to be open, allowing for the exchange of water between the Mediterranean and Atlantic Sea via the Strait of Gibraltar. The bathymetry data for the basins was sourced from the General Bathymetric Chart of the Oceans, GEBCO (https://www.gebco.net/) database. Additionally, a timestep of 360 seconds was used in the simulation.

To compute net fluxes, latent heat, and evaporation, the CORE Bulk formulae was employed (Griffies et al., 2004). The forcing datasets for the model's surface boundary conditions are derived from the ERA5 dataset (Hersbach et al., 2023). This dataset provides the necessary atmospheric forcing fields, including the zonal and meridional components of wind speed at a height of 10 m above the surface (m/s), air temperature (K) and specific humidity (kg/kg) at a height of 2 m above the surface, incoming shortwave and longwave radiation (W/m²), total precipitation (mm/day), and mean sea level pressure (Pa). River runoff data used in this study is obtained from the Global Runoff Data Centre (GRDC) database.

The model incorporates various surface diagnostics, including Sea Surface Temperature (°C), Sea Surface Salinity (psu), Mixed Layer Depth (defined by Sigma

T) (m), Net Downward Heat Flux (W/m²), Latent and Sensible Downward Heat Flux (W/m²), Downward Heat Flux from E-P (W/m²) and Evaporation over open ocean (kg/m^2/s). In addition, depth-resolved diagnostics consist of Sea Water Potential Temperature (°C), Sea Water Potential Salinity (psu), and Vertical Eddy Viscosity (m/s).

The PISCES model was coupled to NEMO through the TOP component in the framework of the study by Karagiorgos et al. (2023). This component handles the advection and diffusion equations of passive tracers, and also manages the sources and sinks associated with biogeochemical processes. In this regional configuration, both the physical and biogeochemical aspects run simultaneously, utilizing an "on-line" coupling approach. Furthermore, both the physics and biogeochemistry components operate at the same high-resolution of 1/12° in the horizontal domain. The open boundary conditions in the Atlantic Ocean and the initial values for biogeochemical variables, excluding DIC (Dissolved Inorganic Carbon) and Alkalinity, are derived from monthly climatology of a Global Ocean Analysis Product (GLOBAL_ANALYSIS_FORECAST_BIO_001_028) provided by Copernicus Marine Service. These boundary and initial conditions are constructed using data at a higher horizontal resolution of 1/4°. To construct the climatology, data from the years 2000 to 2020 is utilized.

Climatological data for DIC and Alkalinity is obtained from the GLODAP v2 dataset, accessible through the NOAA (National Oceanic and Atmospheric Administration) website. A spin-up period of 20 years is conducted through hindcast simulation to establish the starting date of the simulation, which is set as January 1, 2008. This spin-up period allows the model to reach a stable state before the actual simulation commences.

In addition to the open boundary conditions, there are other external inputs that contribute to the nutrient and carbon supply within the model. These inputs originate from three different sources. Firstly, the model accounts for atmospheric dust deposition of elements such as iron (Fe), silicon (Si), phosphorus (P), and nitrogen (N) onto the ocean surface (Aumont et al., 2015). Secondly, river discharges of nutrients are incorporated using the Global NEWS 2 dataset (Mayorga et al., 2010). These nutrient inputs are introduced to the model as surface runoff along the coastlines, reflecting the influence of riverine contributions.

2.4 Experimental design

In this study, two different experiments are examined, spanning a duration of 5 years (2008 - 2012), simulating the Mediterranean and Black Sea waters. Firstly, a reference experiment (REF) was performed in the study of Karagiorgos et al. (2023) replicating the actual environmental conditions observed in the area of interest. To highlight the impact of BSW in the eastern Mediterranean, we modified the model domain of REF experiment to perform an additional experiment (EXP) where the Dardanelles Strait was closed off within the model domain (i.e., no water exchange between the Aegean and the Black Sea). Apart from the previously noted distinction of the Dardanelles Strait, all other aspects (e.g. atmospheric forcing and initial conditions) of the model configuration remain identical for both experiments (i.e., twin-experiment). All the simulations were performed at ARIS High-Performance Computing (HPC) system (*https://www.hpc.grnet.gr/en/)*.

We concentrate our investigation on the North Aegean Sea, particularly within the region defined by coordinates 38.5°N – 41.0°N and 22.5°E – 27.0°E (**Figure 1)**. The focus in this area is motivated by the fact that this region is the initial recipient of BSW and thus undergoes the most significant changes after a 5-year simulation. To examine the impact of BSW on the Aegean and the entire eastern Mediterranean and avoid random results, we would need more extended simulation runs of at least 10 years.

2.5 Mean transport fluxes in Dardanelles

To gain a comprehensive understanding of the factors contributing to the divergences observed in the results of the two experiments - presented in Chapter 3 -, we consider the transport fluxes in the Dardanelles that occurred from 2008 to 2012, as depicted in **Figure 3**.

(a).

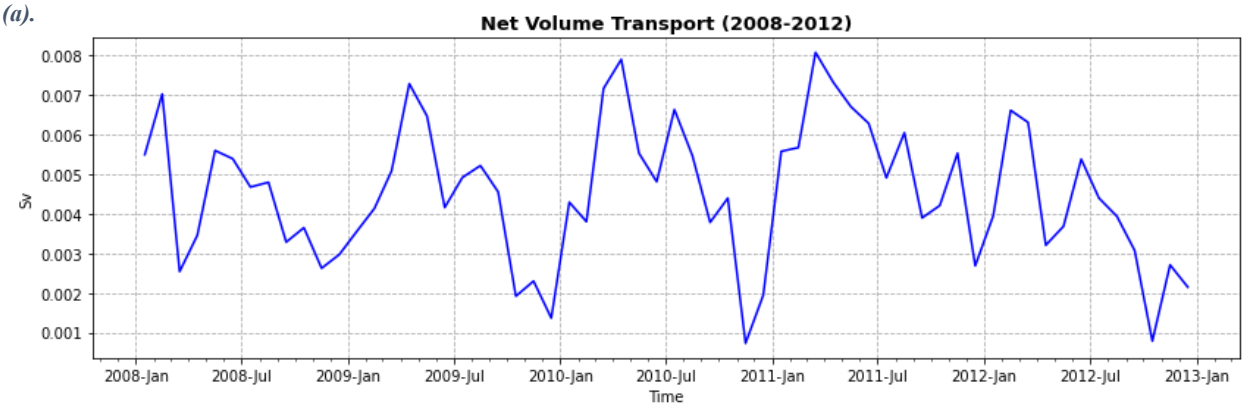
Net Volume Transport (2008-2012)
Sv
0.008
0.007
0.006
0.005
0.004
0.003
0.002
0.001
2008-Jan
2008-Jul
2009-Jan
2009-Jul
2010-Jan
2010-Jul
2011-Jan
2011-Jul
2012-Jan
2012-Jul
2013-Jan
Time

(b).

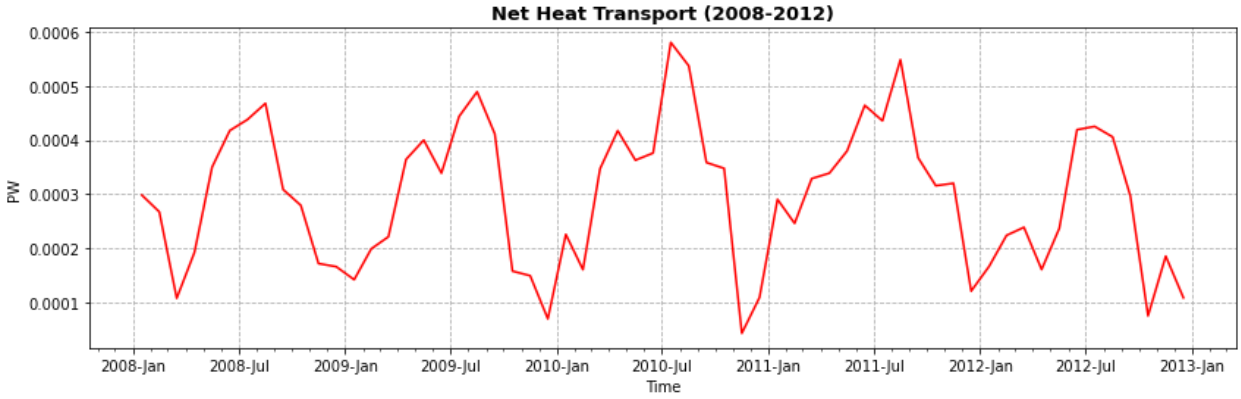
Net Heat Transport (2008-2012)
PW
0.0006
0.0005
0.0004
0.0003
0.0002
0.0001
2008-Jan
2008-Jul
2009-Jan
2009-Jul
2010-Jan
2010-Jul
2011-Jan
2011-Jul
2012-Jan
2012-Jul
2013-Jan
Time

(c).

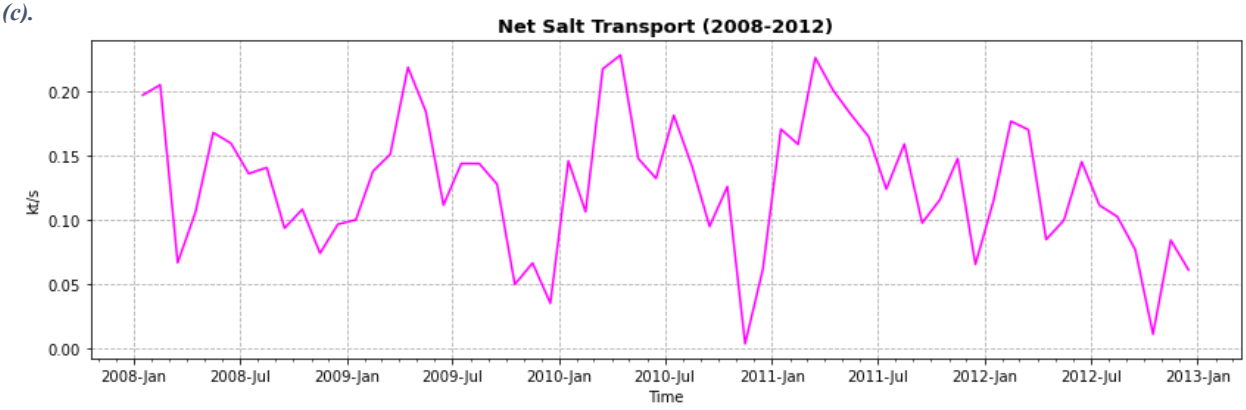
Net Salt Transport (2008-2012)
kt/s
0.20
0.15
0.10
0.05
0.00
2008-Jan
2008-Jul
2009-Jan
2009-Jul
2010-Jan
2010-Jul
2011-Jan
2011-Jul
2012-Jan
2012-Jul
2013-Jan
Time

(d).

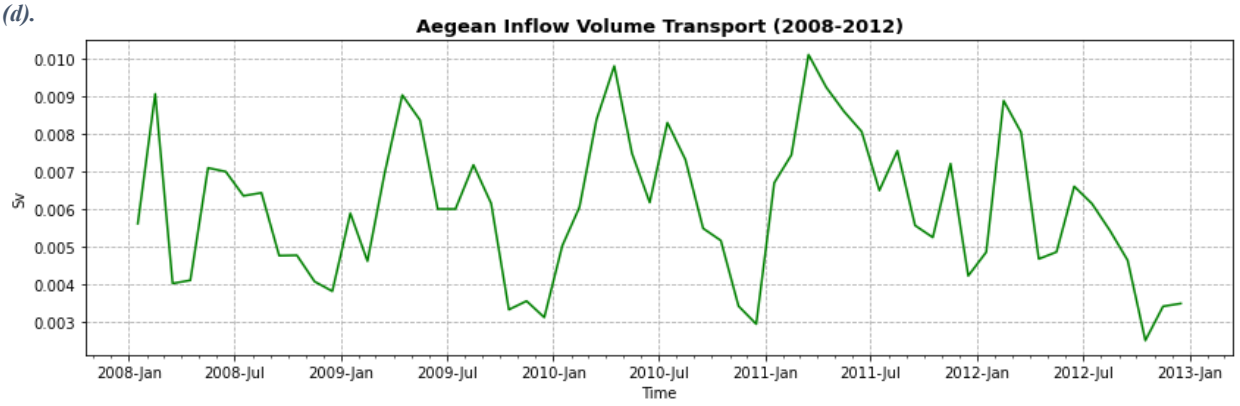

(e).

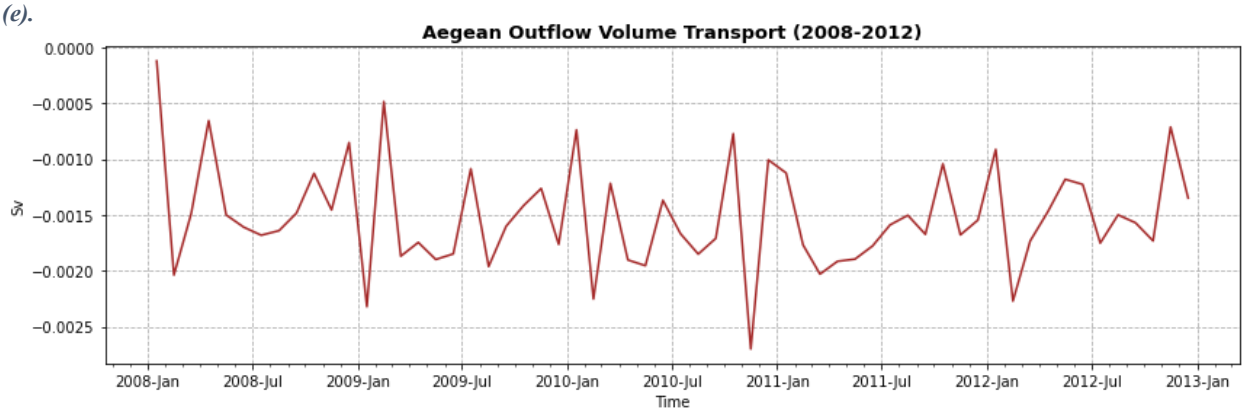

***Figure 3**: **(a)** Net Volume Transport, **(b)** Net Heat Transport, **(c)** Net Salt Transport, **(d)** Aegean Inflow Volume Transport and **(e)** Aegean Outflow Volume Transport occurred from 2008 to 2012 in Dardanelles.*

Chapter 3

Results

In this chapter, we present the results specifically pertaining to the final year (2012) of the experiment, highlighting the seasonal alterations observed within the study region following the completion of the five-year twin experiment. The outcomes from the North Aegean experiment for the fourth and fifth years exhibited significant similarity, implying that the simulation duration is sufficient for analyzing seasonal trends. The examination and analysis of the subject matter were approached from both temporal and spatial perspective, focusing on various upper-ocean and vertical thermohaline and biogeochemical variables during the final year (2012) of the study.

It is important to mention that the anomaly maps and time series displayed in this chapter are derived by subtracting the values from the second experiment EXP, which represents the scenario with the closed Dardanelles Strait, from the values of the first experiment REF, which represents the actual conditions. Mathematically, this is expressed as REF – EXP.

3.1 Temporal evolution

In this subsection, the temporal progression of the thermohaline characteristics and the mean Kinetic Energy is presented during the final year of the twin experiment (2012) in the North Aegean (NA).

3.1.1 Thermohaline characteristics

Within this subsection, the provided time series are derived from daily data encompassing the year 2012. Our initial focus centers on the temporal evolution of Sea Surface Salinity (SSS), which emerges as the key characteristic exhibiting the most notable difference between the two experiments.

Figure 4 reveals that the temporal progression of regional mean SSS values in both experiments exhibits a similar pattern from January to August. The REF experiment attains its highest SSS value in February (~39.0 psu), whereas the EXP experiment reaches its peak in late August (~39.4 psu). However, starting from September, the two experiments diverge in their fluctuation pattern. The surface salinity in REF remains relatively stable in general, with only slight increases observed in November, while EXP shows a consistent decrease until the end of the year.

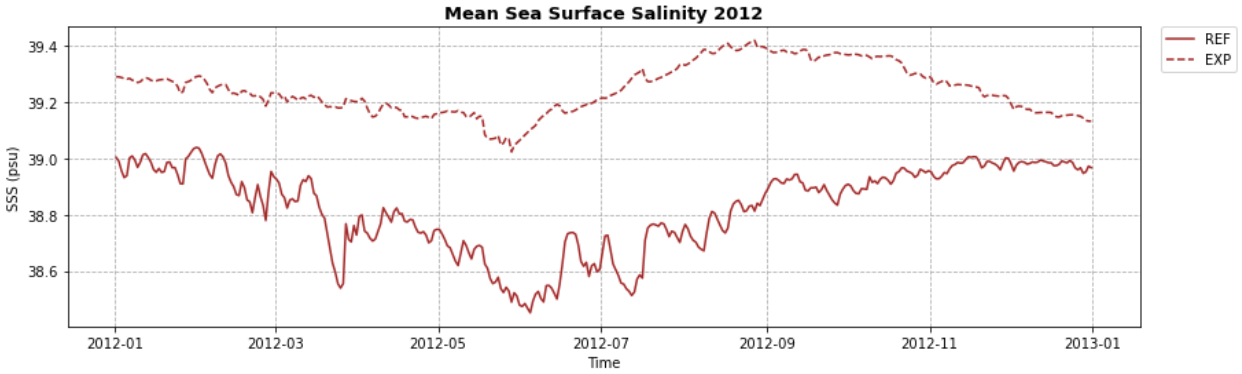

Figure 4: Mean Sea Surface Salinity time series in 2012 for REF (solid line) and EXP (dashed line)

Moving forward, we display the combined time series of mean SSS and SST for both REF (**Figure 5a**) and EXP (**Figure 5b**). In the REF experiment, there exists an almost inverse relationship in the fluctuations of mean SSS and SST. SSS reaches its highest value of approximately 39.0 psu during the winter season, whereas SST reaches its lowest point of 13.6 ºC during the same period. As spring arrives, SST starts to rise while SSS experiences a decline until early June when it reaches its minimum value of 38.45 psu. Between late June and mid-August, both SSS and SST exhibit increasing values. However, afterward, SST shows a tendency to decrease until the end of 2012, in contrast to SSS, which demonstrates an increasing pattern.

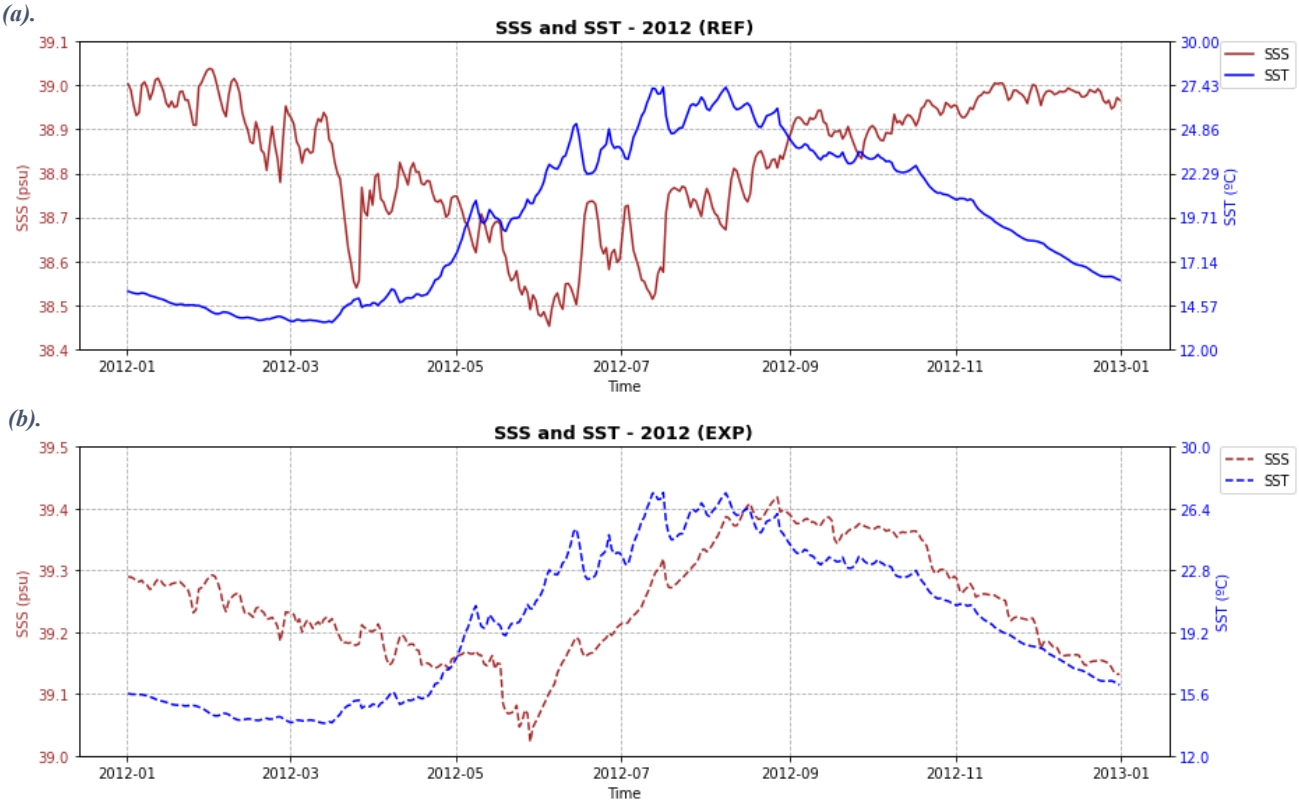

*Figure 5: Daily regional mean Sea Surface Salinity (brown) and Sea Surface Temperature (blue) time series in 2012 for **(a).** REF and **(b)**. EXP.*

On the other hand, **Figure 5b**, which pertains to the EXP experiment, demonstrates a notably similar trend in the fluctuations of mean SSS and SST in the NA. It is evident that both SSS and SST undergo an increase from June to early August. SST reaches its highest value of 27.3 ºC in July, while SSS reaches its peak value of approximately 39.42 psu in late August. However, from late August onwards, both SSS and SST exhibit a decline in their values until the end of the year. Therefore, we conclude that in the hypothetical scenario that EXP represents, there might be a similar pattern in the seasonality of mean SSS and SST fluctuations in the NA, with their peak values being reached during the summer season.

Figure 6 illustrates the mean regional differences in SSS and SST between the two experiments through separate time series. The anomaly between the two experiments reveals a decrease in SSS, indicating that the inflow of BSW into the Aegean Sea reduces the salinity in the region, in accordance with what is already known. Consequently, the hypothetical scenario of a closed DS (EXP) would result in increased salinity within the examined area. This salinity difference is further

highlighted in the SSS anomaly time series, consistently displaying negative values. The difference in SSS values between the two experiments is most pronounced during the summer, reaching a peak mean value of -0.77 psu in mid-July. This can be attributed to the higher BSW inflow that occurs during the summer season (e.g., Beşiktepe et al., 1994; Zodiatis, 1994; Zervakis et al., 2000), leading to an amplified contrast between REF and EXP values. Conversely, the SST anomalies exhibit the most prominent variations from winter to early spring (April), with the highest difference of -0.41 ºC recorded in winter (February). However, starting from May and continuing until the end of the year, the SST difference between REF and EXP remains within the range of -0.1 ºC. The largest reduction in SST in winter can be attributed to the fact that during this specific season mean Kinetic Energy in the NA is significantly reduced (e.g., Tzali et al., 2010), as depicted in **Figure 13a** and **Figure 13c** of subsection 3.2.2. Therefore, the brackish cold waters of Black Sea origin accumulate in NA leading to lower basin-mean SST values, compared to the EXP scenario. Moreover, when comparing the mean SSS with the mean SST anomaly time series, it becomes apparent that they follow similar fluctuations during the winter season.

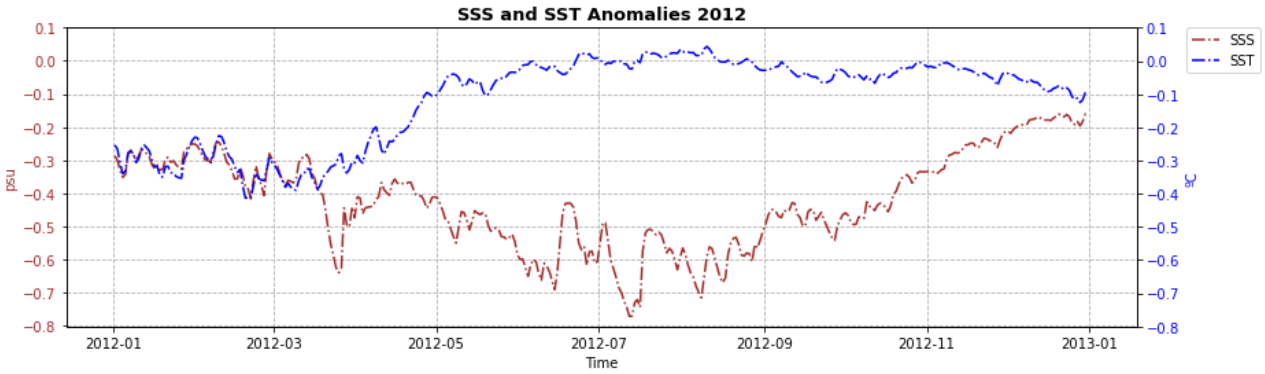

***Figure 6**: Sea Surface Salinity (brown) and Sea Surface Temperature (blue) anomaly time progression in 2012, from daily data. The anomalies are computed as REF – EXP.*

3.1.2 Mean kinetic energy

Figure 7 illustrates the regional temporal evolution of the average Kinetic Energy (KE) during the year 2012. This calculation is based on monthly data and is presented for both the REF experiment (solid line) and the EXP scenario (dashed line). In REF, mean KE reaches its peak of 7.2×10^{-3} m^2/s^2 in August. However, in

the EXP scenario, the highest mean value, which is achieved in June, amounts to 4.2×10^{-3} m^2/s^2. We observe that the mean KE values are greater in the EXP scenario compared to REF, during winter and spring seasons (January to May). Conversely, for the remainder of the year, the KE values in the REF experiment surpass those in the EXP scenario. Therefore, we can conclude that BSW increases the basin-mean KE in summer and autumn, while it decreases its average value during winter and early spring. Additional investigation into the reasons for the fluctuations in KE in each experiment with respect to their seasonal spatial patterns is detailed in subsection 3.2.2.

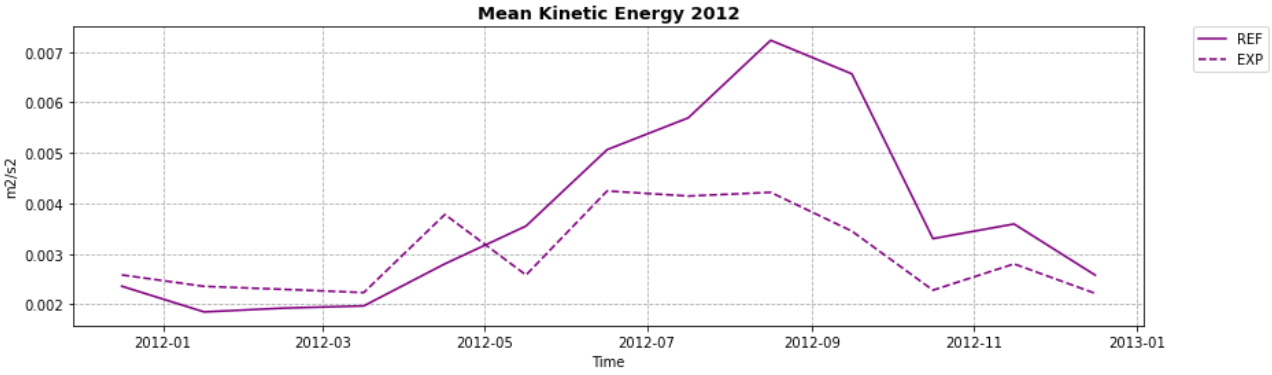

***Figure 7**: Mean Kinetic Energy time series in 2012 for REF (solid line) and EXP (dashed line) scenario.*

3.2 Spatial patterns

In this section, our analysis revolves around the distribution patterns of the model during the winter and summer seasons in the final year of the experiment. We have chosen to concentrate on these seasons due to the significant variations in the inflow of BSW towards the Aegean, with the highest inflow occurring in summer and the lowest in winter, as mentioned in Chapter 1. The winter season encompasses the average values of January, February and March, whereas the summer season comprises the average values of July, August and September. Additionally, alongside the anomaly maps, we also present the corresponding REF maps for a comprehensive understanding of the data. The distinct triangle shape featured in the maps signifies the specific area where the BSW inflow from the DS enters the Aegean Sea.

3.2.1 Thermohaline characteristics

In the final year of the experiment, we calculated the regional mean SSS and SST during the winter and summer seasons. Afterwards, we determined the difference between the values obtained in the EXP and the REF. This allowed us to generate maps illustrating the anomalies in SSS and SST.

Regarding the SSS anomaly map during winter 2012 (**Figure 8c**), there is a significant decrease observed in the northeastern Aegean, particularly in proximity to the region where the BSW enters, reaching a maximum difference of -10.55 psu. The reason behind this result is that when the DS is open (**Figure 8a, 8b**), the lighter, low-salinity BSWs flow into the NA region and tend to remain near the surface, due to their lower density compared to the denser, higher-salinity waters originating from the Levantine region (e.g., Ünlüata et al., 1990; Jarosz et al., 2012).

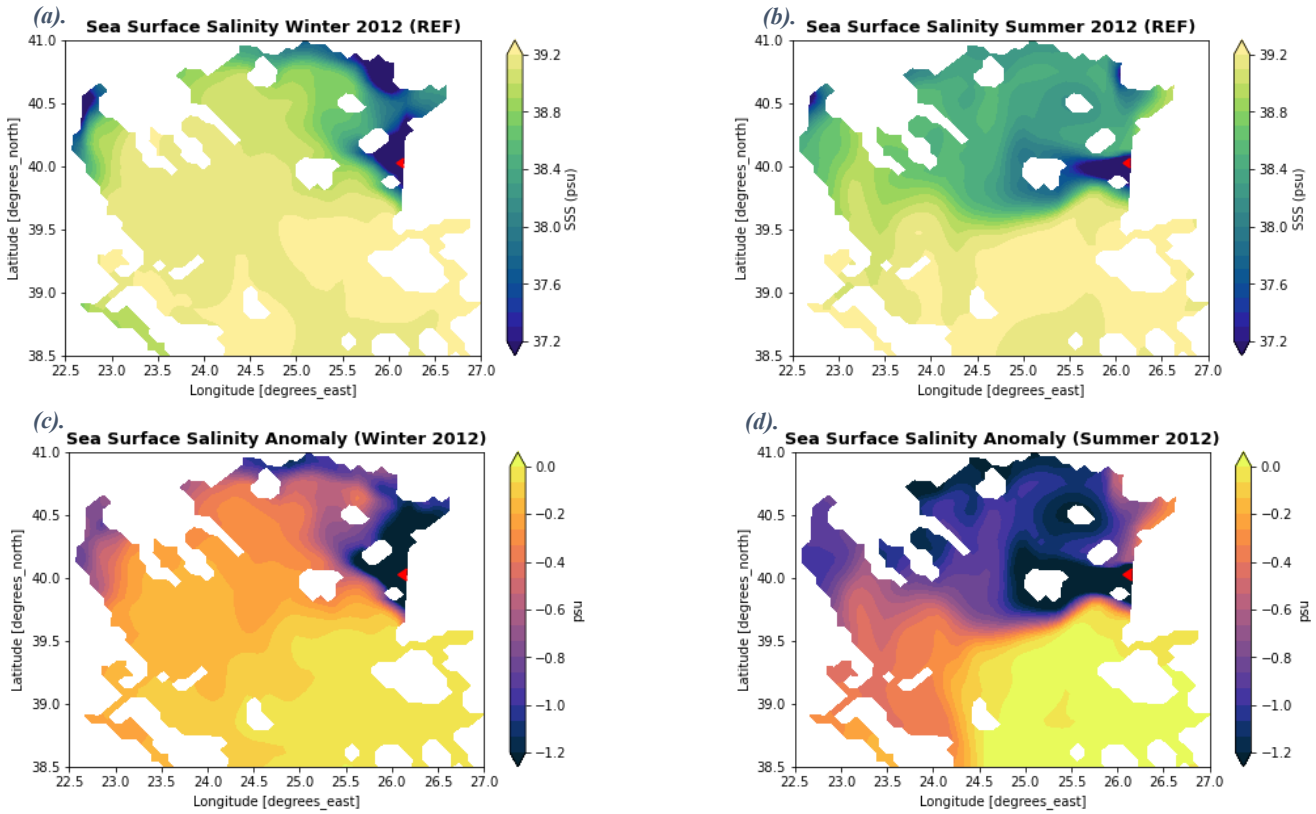

Figure 8: *Mean SSS map in 2012 for* ***(a)*** *REF in winter,* ***(b)*** *REF in summer,* ***(c)*** *the anomaly in winter and for* ***(d)*** *the anomaly in summer.*

In the SSS anomaly map, during the summer of 2012 (**Figure 8d**), we observe a more significant reduction in SSS compared to the winter period, that reaches a maximum difference of approximately -10.97 psu. This decrease extends over a larger area in the NA. As anticipated, this is a result of the increased inflow of low-salinity BSW during the summer season (e.g., Beşiktepe et al., 1994; Zodiatis, 1994; Zervakis et al., 2000). Moreover, the presence of strong north winds during summer (e.g., Kallos et al., 1998) facilitates the spread of the low-saline BSW throughout the northern part of the study region, especially around Limnos and Samothraki Islands. Additionally, it leads to the formation of a pronounced thermohaline front (e.g., Vlasenko et al., 1996) separating the higher salinity Levantine originated waters from the lower salinity waters originating from the Black Sea. It is noteworthy that the SSS anomaly map for summer 2012 (**Figure 8d**) exhibits an anticyclonic formation around Samothraki Island. This can be attributed to the specific circulation patterns of the area, which will be further discussed in subsection 3.2.2.

Figure 9a depicts the variations in mean SST in the NA during the winter of 2012, as simulated in the REF experiment. On the other hand, **Figure 9b** represents the

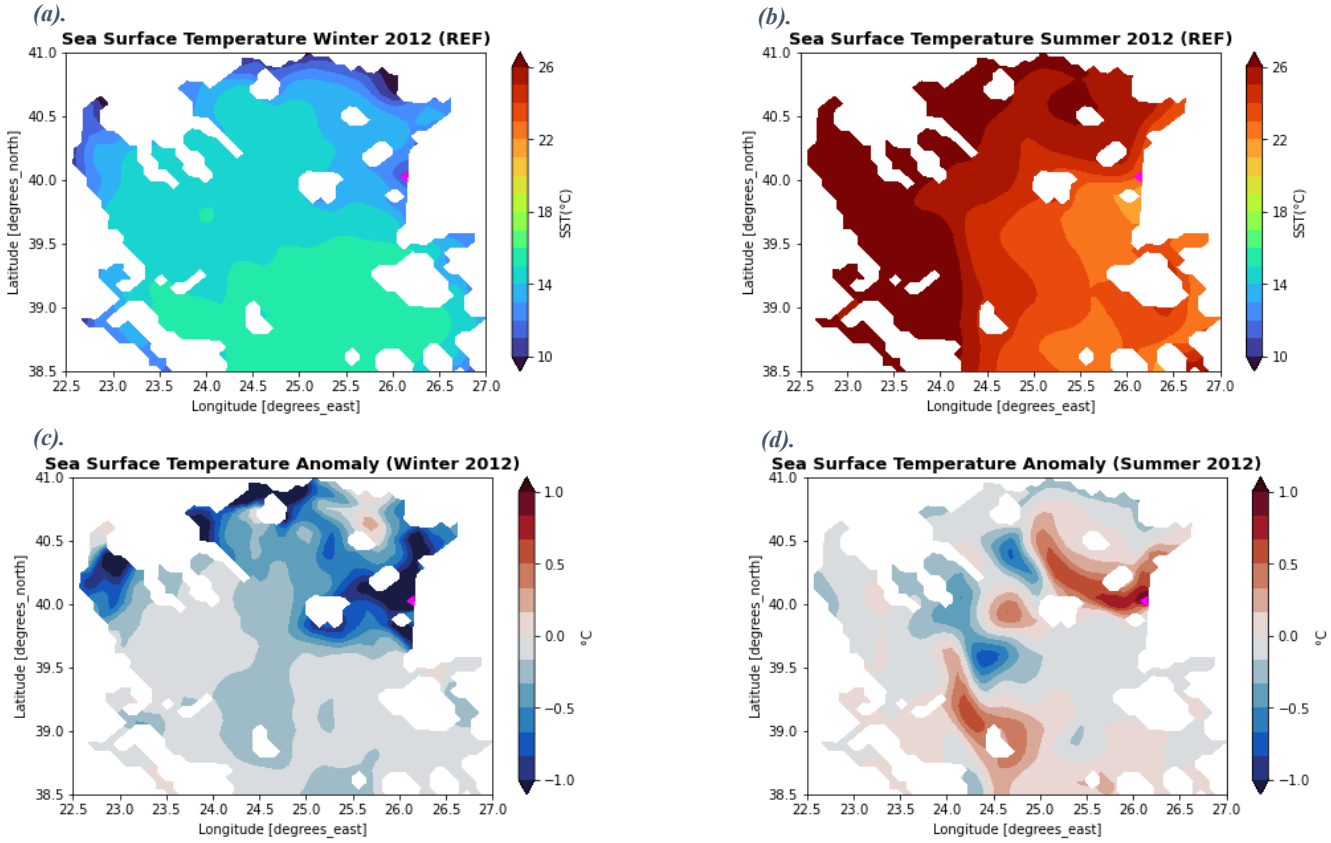

*Figure 9: Mean SST map in 2012 for **(a)** REF in winter, **(b)** REF in summer, **(c)** the anomaly in winter and for **(d)** the anomaly in summer.*

SST patterns for the summer of the same year. A notable observation is that the entire region experiences lower temperatures during the winter months, ranging from 8.7 to 15.8°C, compared to the warmer temperatures in summer, ranging from 21.3 to 28.6 °C. In both seasons, we observe consistently lower SST values near the DS exit area compared to the surrounding regions. This potentially suggests that the BSW tends to have a cooling effect on the SST, regardless of the season. The SST anomaly map for winter 2012 (**Figure 9c**) reveals a decrease in the vicinity of the area where the BSW enters (DS exit). The maximum temperature drop observed amounts to -3.7 °C. In contrast, during summer 2012, we notice a significant rise in SST anomaly map (**Figure 9d**). This rise is also located near the DS exit and expands northwards around Samothraki Island, aligning with the typical circulation pattern of the area. However, this temperature increase does not exceed +1.4 °C. One of the key factors that might have contributed to this SST rise (**Figure 9d**) might be the significant net heat transport levels towards the Aegean Sea (**Figure 3b**), with their highest rate (in 2012) being observed during the summer season. Nonetheless, it would be beneficial to conduct simulation runs over a more prolonged duration (at least 10 years) to investigate the factors contributing to the SST rise depicted in **Figure 9d**.

To examine the density patterns, we extracted zonal cross sections. Following this, we display the representative zonal profiles taken at the geographic latitude (40°N) of the Dardanelles Strait (**Figure 1b**), illustrating depth-wise potential temperature anomaly (**Figure 10**), salinity variations (**Figure 11**), and potential density anomaly (**Figure 12**) in 2012.

There is a noticeable reduction in both temperature and salinity anomalies during the summer, primarily within the upper 30 meters of the water column (**Figure 10b** and **Figure 11b**). However, in the temperature anomaly map (**Figure 10b**), there is also a significant increase between 24.3 ºE and 24.8 ºE. Additionally, during the summer season, the temperature anomaly map (**Figure 10b**) reveals a significant decrease between depths of 200 to 400 m, while the corresponding salinity anomaly map (**Figure 11b**) demonstrates a declining pattern starting from 200 m and extending to 1062 m (seabed).

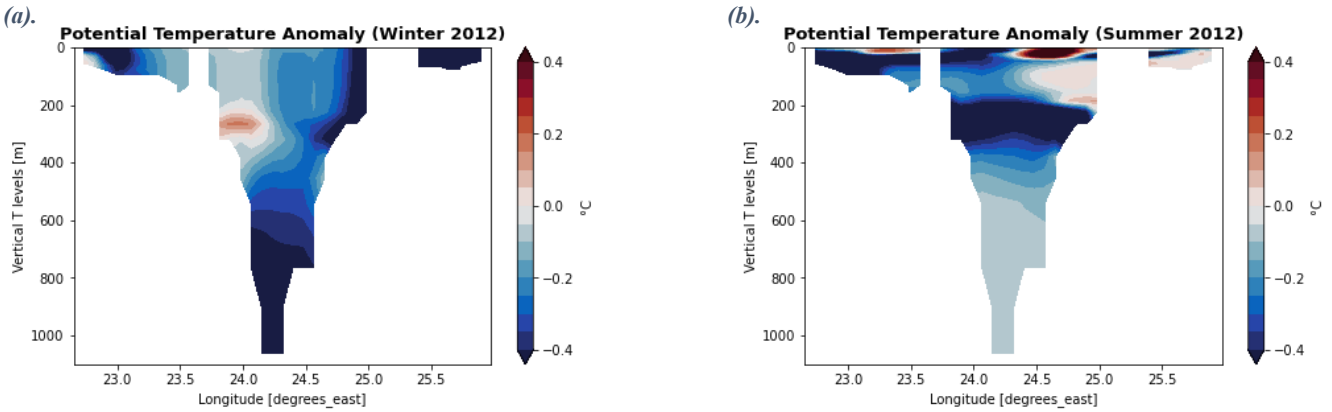

Figure 10: Zonal cross section of sea water potential temperature anomaly at 40°N in **(a)** winter and **(b)** summer 2012.

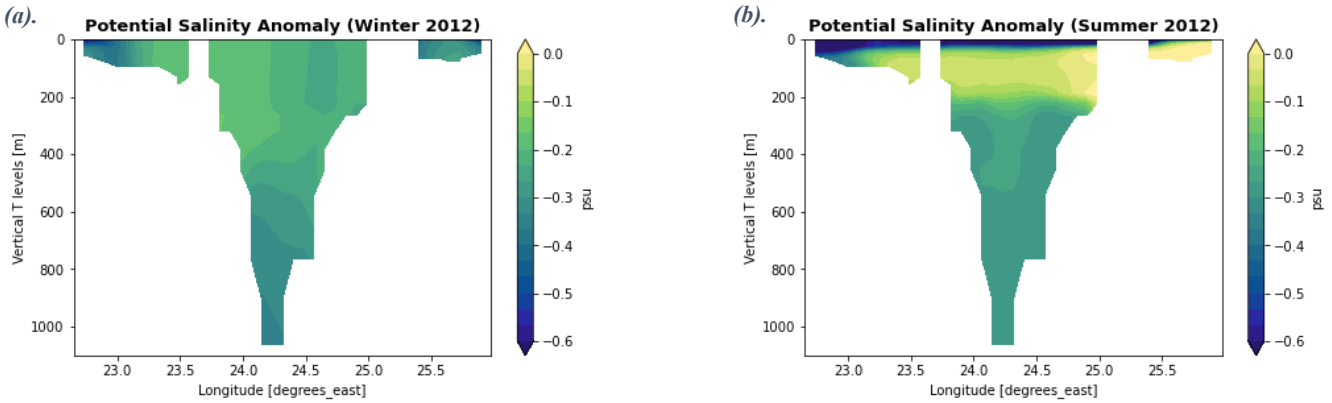

Figure 11: Zonal cross section of sea water potential salinity anomaly at 40°N in **(a)** winter and **(b)** summer 2012.

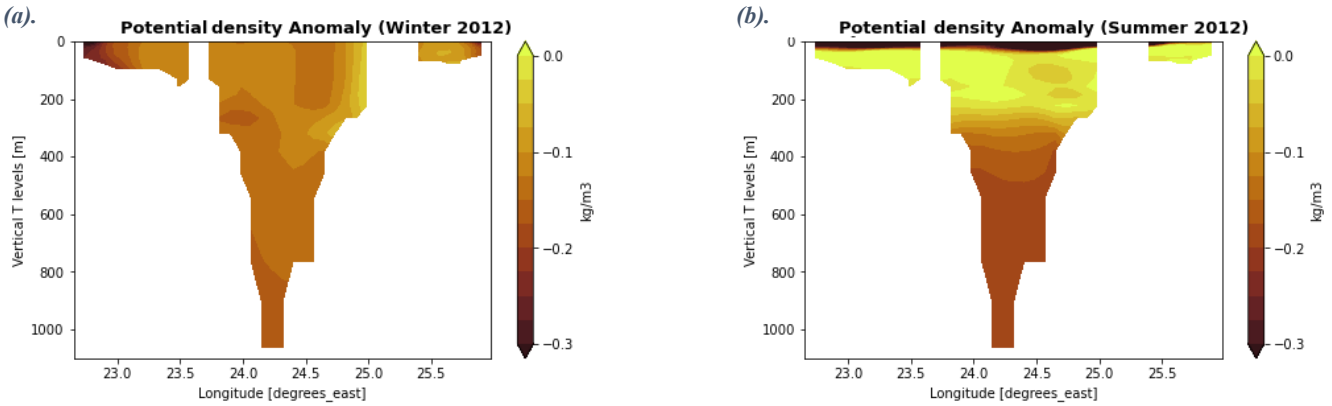

Figure 12: Zonal cross section of potential density anomaly at 40°N in **(a)** winter and **(b)** summer 2012.

In the summer season, the potential density anomaly map (**Figure 12b**) exhibits variations at the same depths as the salinity anomaly map. Similar to the declining pattern observed in the salinity anomaly map, there is a corresponding decrease in the density. The most significant drop recorded, approximately -1.18 kg/m^3, occurs

near the surface. During the summer season, there has been one more significant decline in the density starting from around 250 m and extending to the sea bottom at 1062 m (**Figure 12b**). The most substantial reduction in density observed during this period, at these depths, reached a maximum of -0.2 kg/m^3.

Regarding the potential density anomaly map during the winter season (**Figure 12a**), there is a pattern remaining evident across nearly all depths, from the surface to the bottom. In line with the decreasing pattern noticed in salinity, the density also exhibits a consistent decline in winter. One of the most significant reductions is recorded below 600 m, reaching approximately -0.16 kg/m^3. Hence, it can be inferred that a complete absence of BSW inflow into the Aegean Sea (EXP) would potentially enhance the process of deep water formation. A more extensive elaboration concerning deep water formation processes can be found in subsection 3.3.

3.2.2 Seasonal kinetic energy and annual circulation patterns

There are only a few variations observed between the two experiments when considering the mean Kinetic Energy (KE) during winter 2012, as evident from the corresponding anomaly map in **Figure 13c**. The primary distinction is a slight elevation in KE values moving from the DS exit towards the west, reaching approximately $+4.1\times10^{-2}$ m^2/s^2. The largest value in the mean KE anomaly map during summer 2012 (**Figure 13d**) amounts to approximately $+5.8\times10^{-2}$ m^2/s^2. In both experiments, the positive difference between REF and EXP indicates that the inflow of BSW contributes energy to the North Aegean Sea. An interesting remark is that, once again, during summer 2012, this increase in KE forms a distinct anticyclonic pattern encircling Samothraki Island, aligning with the typical circulation pattern of the region during the summer season (e.g., Zervakis and Georgopoulos, 2002). We can also infer that the simulated rise in KE (depicted in **Figure 13d**) near the DS exit during summer may be correlated with the higher SST values (**Figure 9d**) and the lower SSS values (**Figure 8d**) in the same geographical region. This combination results in a reduction in surface water's density, leading to a more pronounced stratification, consequently trapping the lighter waters near the surface, and enhancing the surface horizontal current speed.

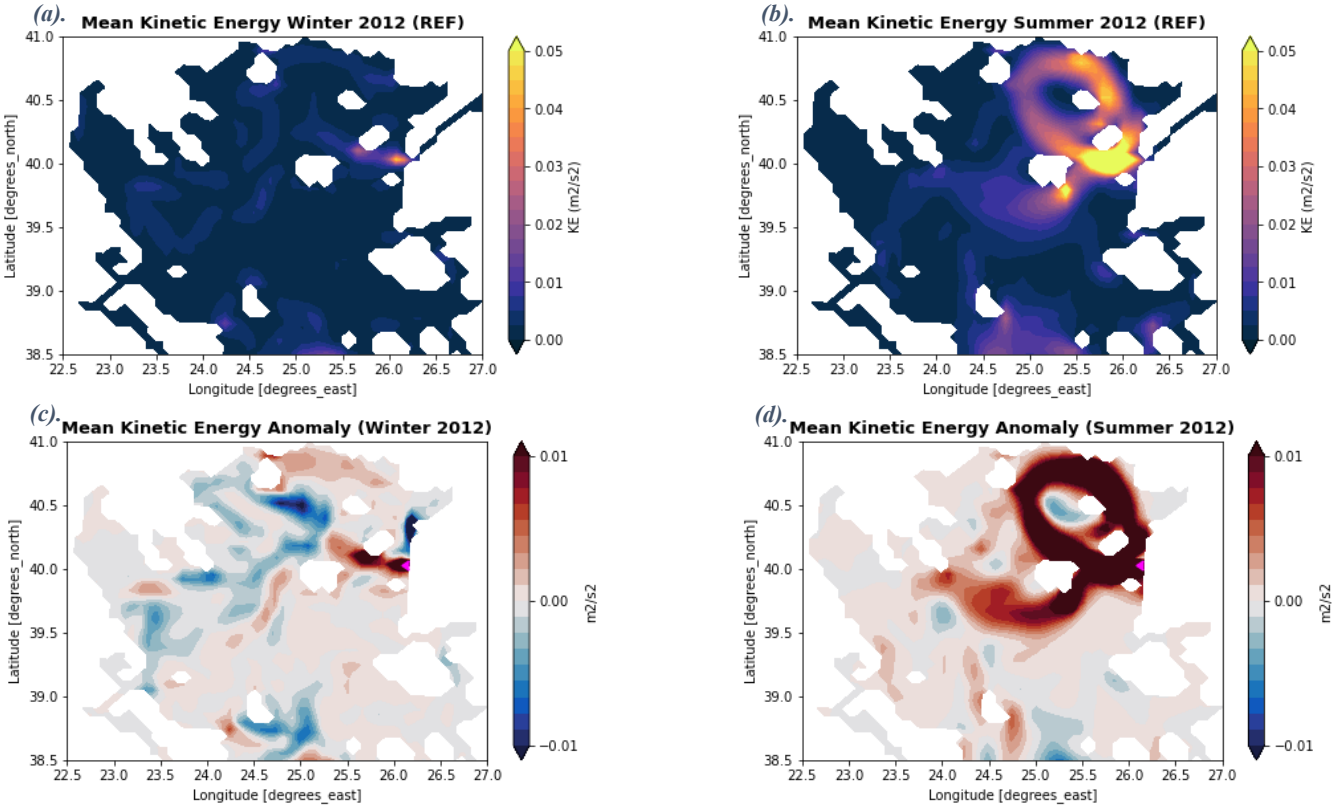

Figure 13: Mean KE map in 2012 for ***(a)*** *REF in winter,* ***(b)*** *REF in summer,* ***(c)*** *the anomaly in winter and for* ***(d)*** *the anomaly in summer.*

Figure 14 and **Figure 15** present the mean annual circulation pattern in the NA for REF and EXP, respectively. Both experiments exhibit the prominent circulation patterns found in the region, including the anticyclonic formation around Samothraki Island and the cyclonic formation in the northern area of the Sporades Islands. However, a notable difference arises in the cyclonic formation near the Sporades Islands in EXP. Specifically, the center of this cyclonic formation has shifted approximately 0.1º southward and 0.2º eastward compared to REF. Moreover, upon contrasting **Figure 14** with **Figure 15**, it becomes evident that the mean velocity values have decreased significantly. The reason behind this phenomenon might lie in this subsection's previous findings, that the inflow of BSW is a significant energy contributor to the North Aegean Sea. Consequently, the lack of BSW inflow (as in EXP), leads to a weakening of mesoscale cyclonic and anticyclonic eddies (**Figure 15**).

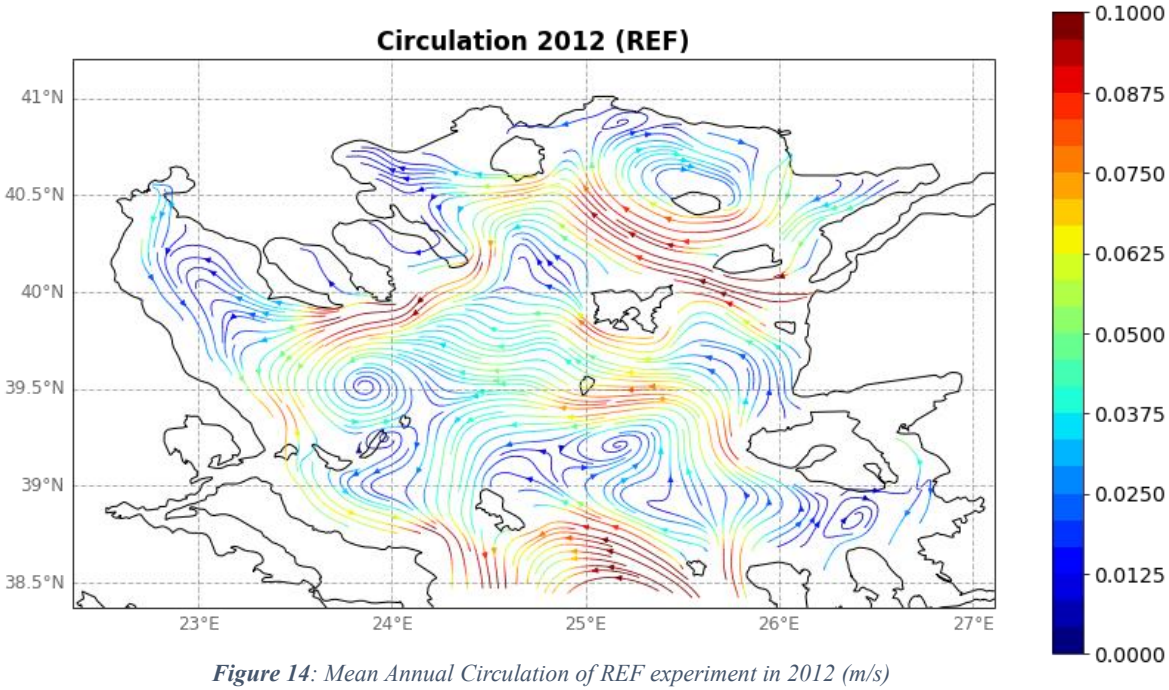

***Figure 14**: Mean Annual Circulation of REF experiment in 2012 (m/s)*

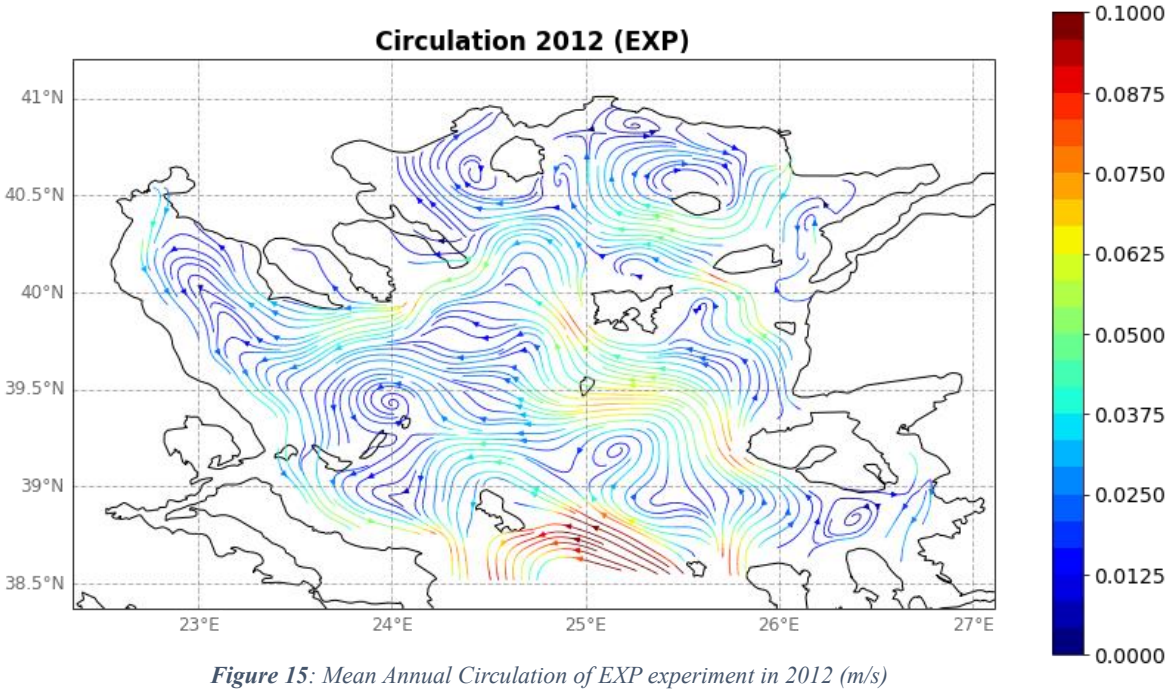

***Figure 15**: Mean Annual Circulation of EXP experiment in 2012 (m/s)*

3.3 Deep water formation

In the introduction (Chapter 1), it was stated that a combination of winter cooling temperatures, rising salinity levels, and decreased outflow of BSW in the Aegean Sea are believed to be contributing factors in the formation of dense water in the region. These factors were crucial in triggering the occurrence of the Eastern Mediterranean Transient (EMT) between 1987 and 1993 (Zervakis et al., 2000; Nittis et al., 2003; Lascaratos et al., 1999; Theocharis et al., 1999; Stratford and Haines, 2002).

In this subsection, our attention is directed towards exploring the potential occurrence of dense water formation processes in the Aegean Sea. We aim to investigate this possibility under the hypothetical scenario presented in EXP, where there is an absence of BSW inflow into the study area. As a result, our analysis centers on studying anomalies observed in variables such as the Mixed Layer Depth, potential density and oxygen levels in the winter season of 2012.

3.3.1 Mixed layer depth

In **Figure 16a** and **Figure 16b**, we present the average seasonal Mixed Layer Depth (MLD) for both the REF and EXP experiments, during the winter of 2012. It is evident that within the central and western sectors of the study area, the mixed layer extends to greater depths in the REF experiment compared to the EXP scenario. Specifically, the maximum depth of the MLD in REF reaches 554.2 m, while in EXP, it attains a peak value of 371.7 m. However, between the Samothraki and Imbros Islands region, EXP exhibits a noteworthy deepening of the MLD in contrast to REF. It's worth noting that this is also the region where the most significant changes between the two experiments are observed, regarding thermohaline characteristics (subsection 3.2.1).

The average seasonal differences between the two experiments are summarized in **Figure 16c**, where the most significant difference amounts to +310.6 m. This positive anomaly indicates that the BSW inflow leads to a deepening of the MLD

across the largest part of the North Aegean. Conversely, an analysis of the anomaly map (**Figure 16c**) reveals that BSW inflow also results in a shallower MLD between the Samothraki and Imbros Islands, as well as northwesterly of the Dardanelles Strait exit, reaching a maximum elevation of -201.1 m. It's worth noting that these areas in the EXP scenario, where MLD deepening occurs, could potentially be sites for deep water formation. Additionally, in **Figure 16c**, we observe that regions where MLD is in deeper depths correspond to regions where a decline in mean surface KE is evident (**Figure 13c**). This observation is consistent with the concept that areas featuring deeper MLD tend to mitigate the impact of wind on the surface layers, consequently leading to a decrease in surface KE.

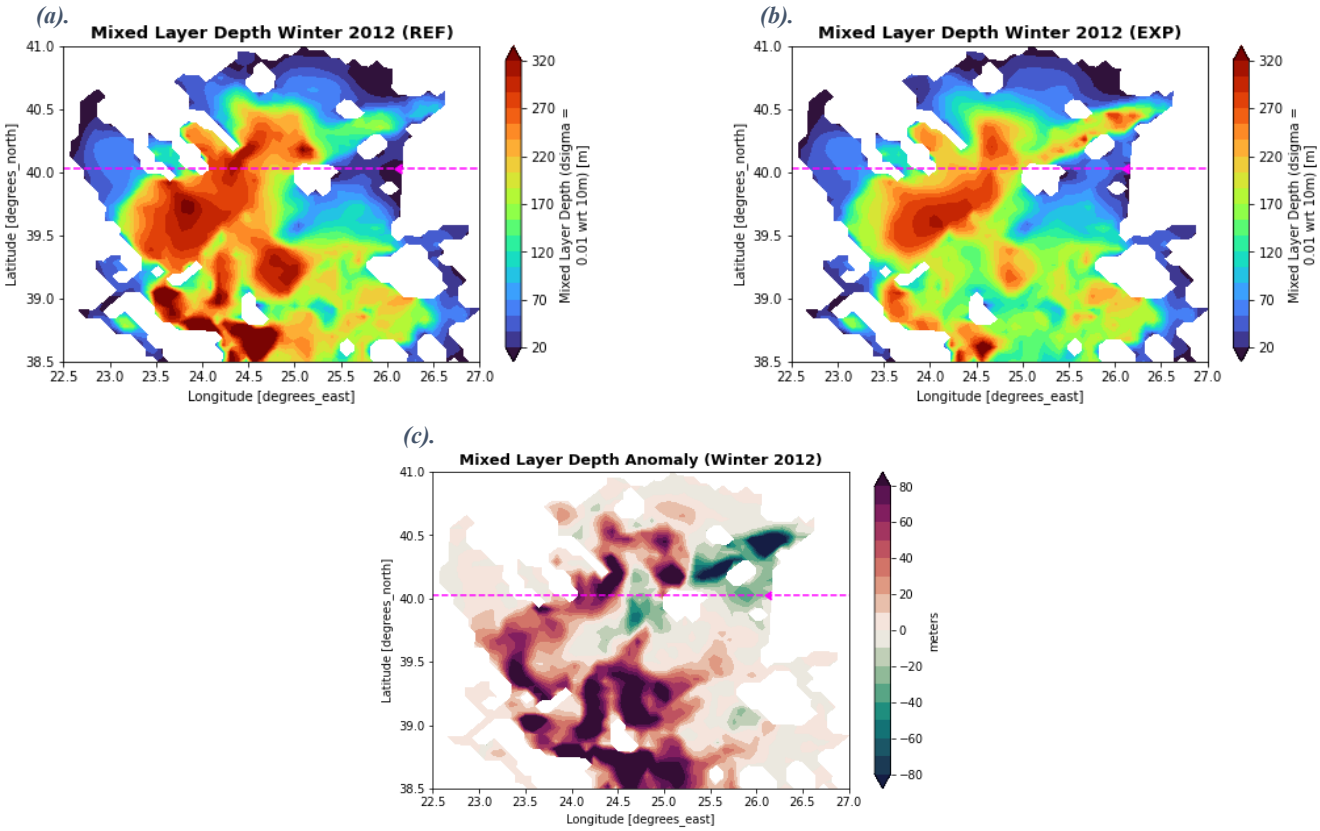

***Figure 16**: Mixed Layer Depth map in winter 2012 for **(a)** REF, **(b)** EXP and **(c)** for the anomaly of the two experiments (REF – EXP). The dashed line indicates the location that we performed zonal cross sections in the following subsections.*

3.3.2 Zonal cross sections of potential density

As demonstrated in subsection 3.2.1, our results indicate that the alterations in potential density are primarily driven by changes in salinity. This relationship is exemplified by **Figure 11** and **Figure 12**, which display similar patterns of anomalies between salinity and density. Consequently, the influence of SST changes is of secondary importance for our analysis in this subsection.

Figure 17a and **Figure 17b** present representative zonal profiles captured at a geographical latitude of 40°N, specifically in the winter of 2012. These profiles depict the potential density in the REF and EXP cases, respectively. It is important to note that in winter 2012 the potential density in EXP (**Figure 17b**) reaches higher values compared to REF (**Figure 17a**) throughout the depth range. In **Figure 17c**, we showcase the anomaly between these two scenarios. Upon analysis, it is apparent that in the REF case, the potential density remains below 29.37 kg/m^3 within the depth range of 300 m to 1062 m (seabed). Conversely, in the EXP case, the potential

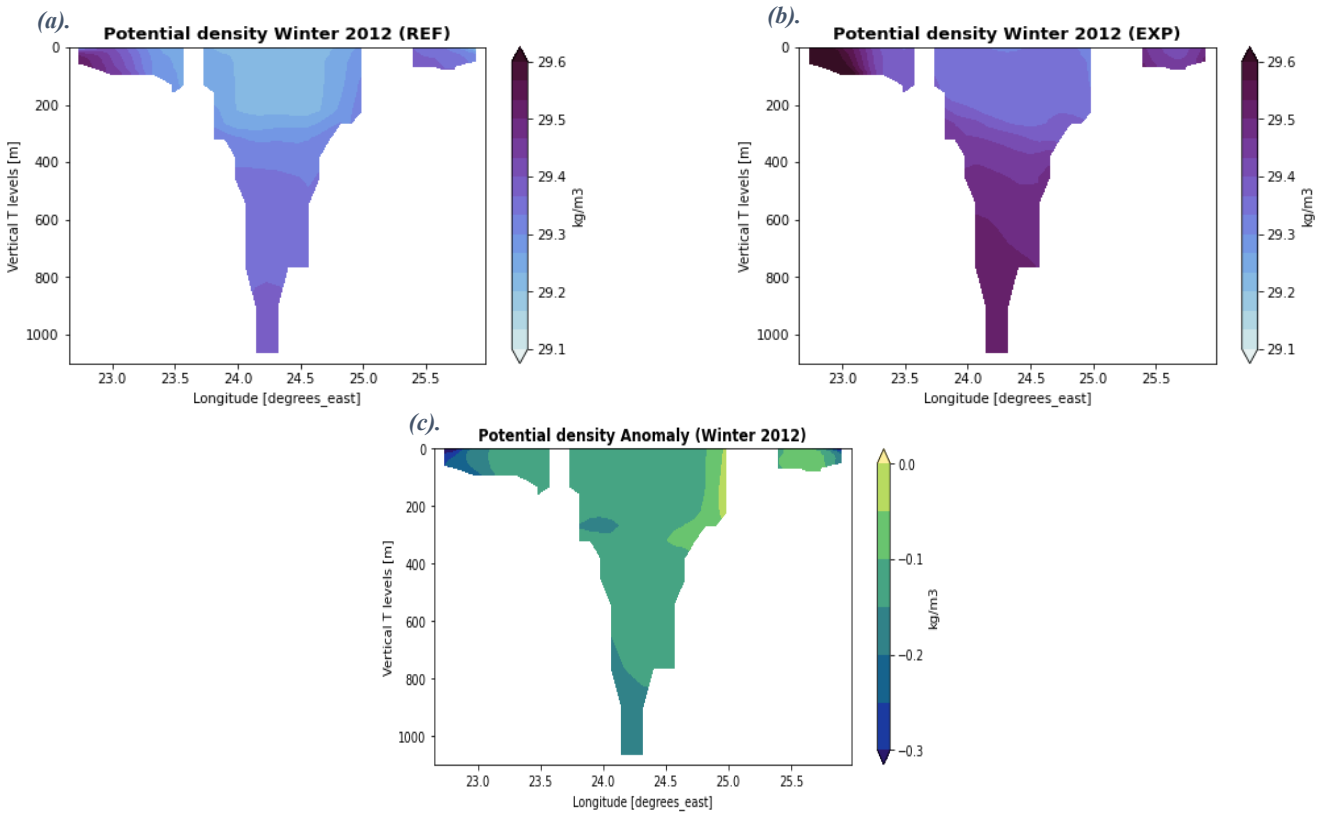

*Figure 17: Zonal cross sections at 40°N of potential density in winter 2012 for **(a)** REF, **(b)** EXP. **(c)** Anomaly of the two experiments (REF – EXP).*

density notably increases, reaching approximately 29.53 kg/m^3 within the same depth range. Consequently, the anomaly map indicates a decrease of approximately -0.16 kg/m^3 in these depths, which is the prevailing anomaly across the entire domain.

In the case of REF, brackish water's presence on the surface has been noted to exert a substantial influence on the deep water formation processes in the region. This surface layer of brackish water acts as a barrier, inhibiting the development of water masses below it (e.g., Vervatis et al., 2013). Hence, it can be inferred that the absence of BSW inflow (EXP) plays a crucial role in enhancing deep water formation. Upon further analysis of **Figure 17b** and **Figure 17c**, it is possible to suggest that the increased potential density levels observed at depths exceeding 700 m may be attributed to the sinking of dense surface water. This could be a consequence of the SSS levels rise (in EXP), leading to denser surface waters and therefore, enhancing sinking processes, during the initial years of the experiment. To verify this process, we analyze and quantify the corresponding oxygen levels maps, in subsection 3.3.3.

3.3.3 Zonal cross sections of oxygen levels

In addition to the potential density depth-wise zonal profiles, we showcase the corresponding profiles for oxygen levels in REF (**Figure 18a**) and EXP (**Figure 18b**) experiments. We can observe a noticeable rise in oxygen levels within the depth range of around 30 to 300 meters in the EXP scenario. However, the most significant difference between the two experiments becomes evident when examining the oxygen anomaly map (**Figure 18c**), particularly below 400 meters, which shows that oxygen levels are significantly decreased, reaching a peak difference of -11.83 mmol/m^3. Therefore, it can be inferred that in EXP oxygen levels are notably increased in these depths. The presence of augmented oxygen levels in great depths could be the result of surface oxygen-rich waters sinking, leading to deep water formation processes, which further supports the idea presented in subsection 3.3.2.

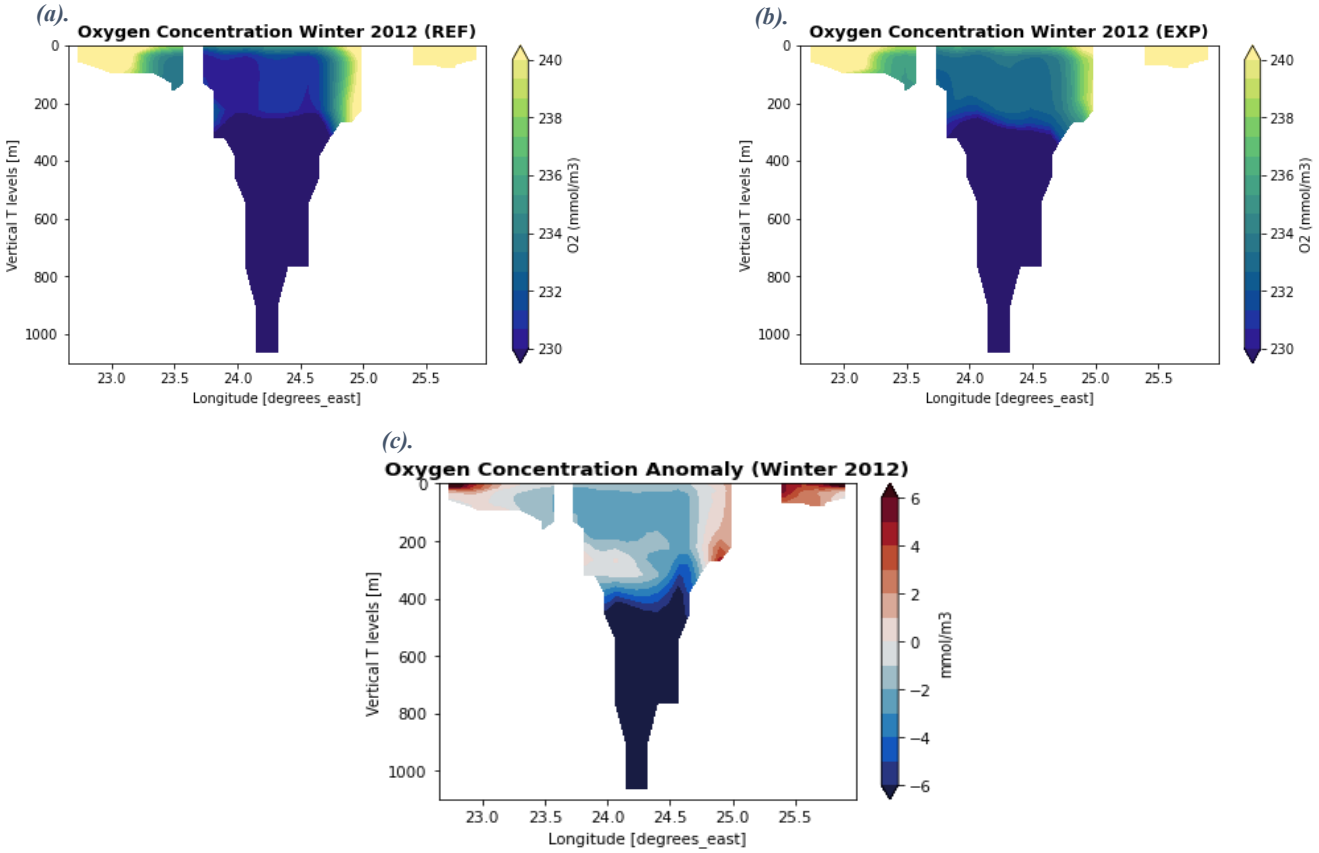

***Figure 18**: Zonal cross sections at 40°N of oxygen concentration in winter 2012 for **(a)** REF, **(b)** EXP. In **(c)** the anomaly of the two experiments is presented (REF – EXP).*

3.4 Biogeochemical characteristics

In the upcoming subsection, we analyze the spatial and temporal variations observed between the two experiments (i.e., REF and EXP) concerning the mean levels of chlorophyll, oxygen, inorganic nutrients (nitrate, phosphate, silicate), and carbonate system variables (alkalinity, DIC), in addition to their mean annual average vertical profiles.

3.4.1 Seasonal spatial patterns

In this subsection, we examine the spatial variations in chlorophyll and oxygen concentrations within the NA region, specifically during the winter season, which includes the significant month of March. This particular month is of great importance due to its known high frequency of blooming events. Our research will primarily compare the chlorophyll and oxygen concentrations of the two experiments during this critical period, through the corresponding seasonal anomaly maps that are presented in **Figure 19b** and **Figure 20b**, respectively.

Upon examining **Figure 19a**, we note a significant rise in mean surface chlorophyll concentration close to the exit of the Dardanelles Strait, as well as in the coastal zones where rivers discharge. The intensified concentration near the Dardanelles Strait extends towards the northeast and attains its highest value of 3.39 gChl/m^3.

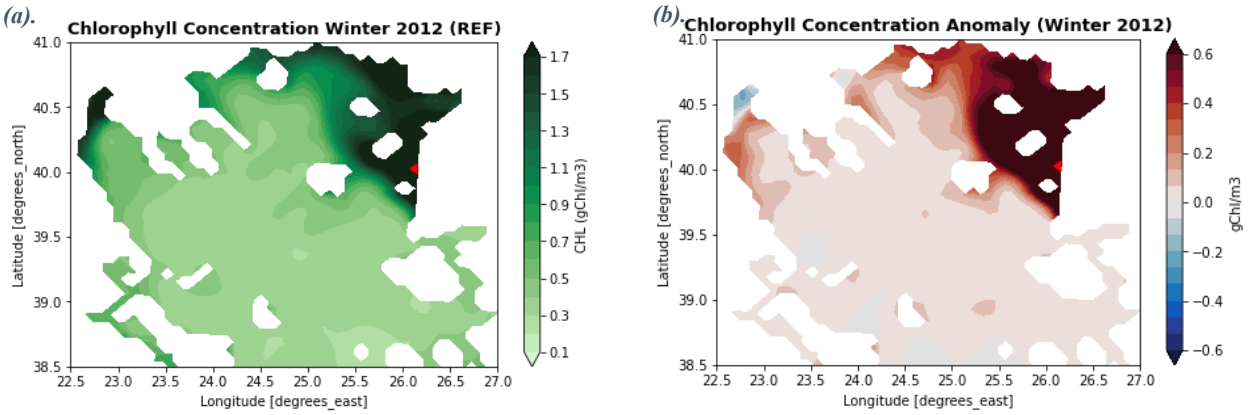

*Figure 19: Mean surface chlorophyll map in winter 2012 for **(a)** REF and for **(b)** the anomaly.*

Turning to **Figure 19b**, the anomaly between the outcomes of the two experiments in this specific area is notably increased, reaching an approximate difference of +2.97 gChl/m^3. This leads us to the conclusion that the presence of BSW contributes to heightened surface chlorophyll levels within the region, while they are substantially diminished in the EXP scenario.

In **Figure 20a**, we illustrate the seasonal mean surface oxygen concentration in the NA for the REF scenario. As we examine the map, it becomes evident that surface oxygen levels are increased in proximity to the exit of the Dardanelles Strait, as well as along the coastal zones where river outflows occur. Notably, the oxygen concentration attains its peak value at 294.52 mmol/m^3. **Figure 20b** displays the oxygen anomaly near the surface, providing the variation between the two experiments.

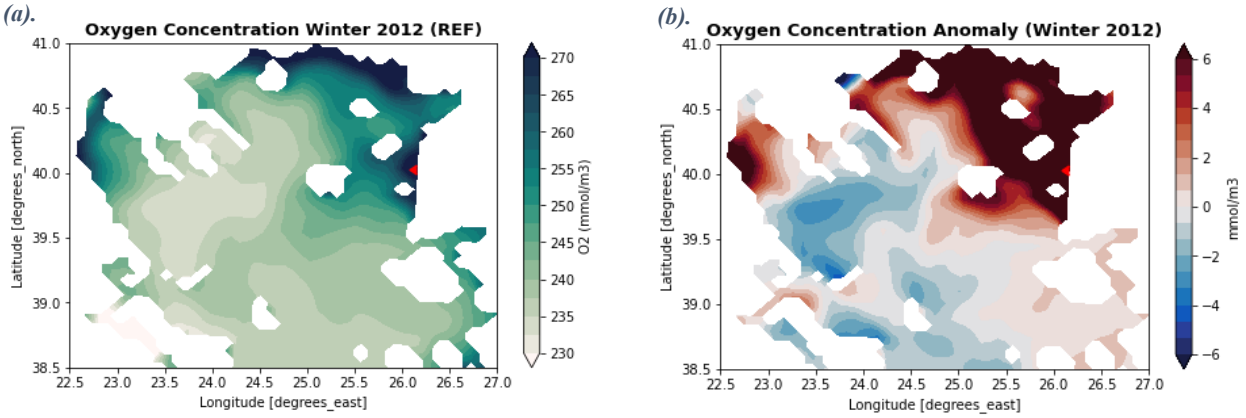

*Figure 20: Mean surface oxygen concentration map in winter 2012 for **(a)** REF and for **(b)** the anomaly.*

Similar to the map depicting the anomaly in surface chlorophyll concentration (**Figure 19b**), the oxygen anomaly map highlights a rise in the vicinity of the Dardanelles Strait exit, where BSW discharges. This increase reaches a value of +43.72 mmol/m^3. Nevertheless, it's worth noting a slight decline in oxygen levels in the western portion of the study region, between 39.3ºN - 39.9ºN and 23.3ºE – 23.7ºE, with a reduction of approximately -3.5 mmol/m^3, which means that BSW inflow reduces surface oxygen levels in this specific area. The reason for this decline can be linked to the strengthened cyclonic circulation pattern in the vicinity of Sporades Islands, which is intensified by the BSW (**Figure 14**), as discussed in subsection 3.2.2. This rise enhances the vertical mixing process, potentially causing

the upper layer of oxygen-rich water to sink and resulting in reduced oxygen levels at the surface in the western part of the region.

3.4.2 Temporal evolution

The temporal variation of regional mean chlorophyll concentration in 2012 is depicted in **Figure 21** for both experiments. It is notable that March stands out as the month when both experiments reach their peak chlorophyll concentrations, which can be attributed to the seasonal chlorophyll bloom occurrence during this period. In the REF experiment, the maximum value recorded is 1.07 gChl/m^3, while in the EXP scenario, it is lower at 0.67 gChl/m^3. The lowest chlorophyll concentration in REF occurs in summer (August), reaching a value of 0.25 gChl/m^3. On the other hand, in the EXP experiment, the minimum concentration is observed in the summer month of July, reaching 0.17 gChl/m^3. Thus, we can infer that BSW increases the basin-mean surface chlorophyll concentration. Despite the differences in values, both experiments display comparable patterns of mean chlorophyll concentration fluctuations throughout the year.

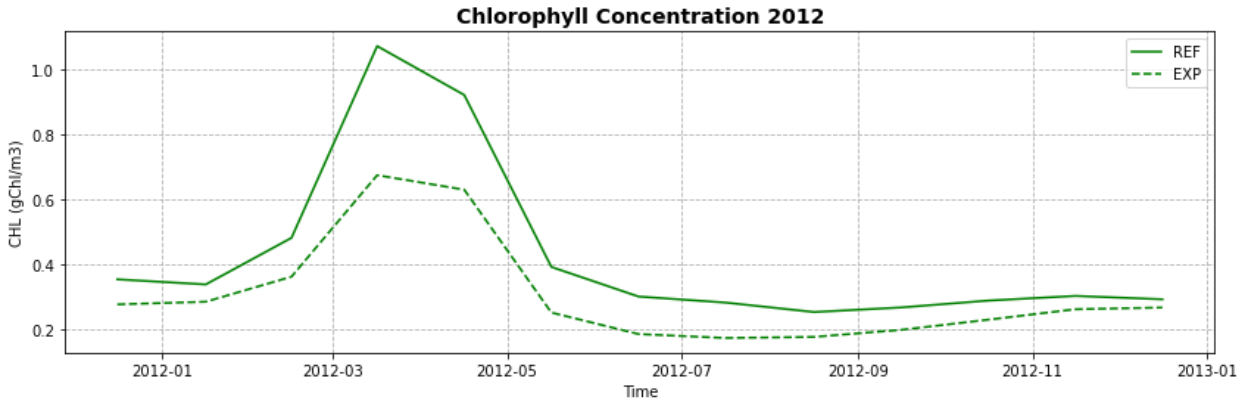

***Figure 21**: Temporal evolution of mean surface Chlorophyll concentration in 2012 for REF (solid line) and EXP (dashed line) in the North Aegean Sea.*

Figure 22 illustrates the regional mean surface oxygen concentration levels for both REF and EXP experiments in 2012. Both experiments exhibit comparable fluctuation patterns throughout the year, although the oxygen values in EXP consistently remain lower than those in REF. During August, both REF and EXP reach their respective minimum values, with REF measuring 214.1 mmol/m^3 and

EXP lower at 212.4 mmol/m^3. Furthermore, the maximum oxygen concentration in REF occurs in April, reaching a value of 255.6 mmol/m^3, while in EXP, the maximum value is lower at 251.1 mmol/m^3, also recorded in April. Despite these differences in values, both experiments demonstrate similar seasonal variations in oxygen levels. Hence, we can conclude that BSW raises the basin-mean surface oxygen values.

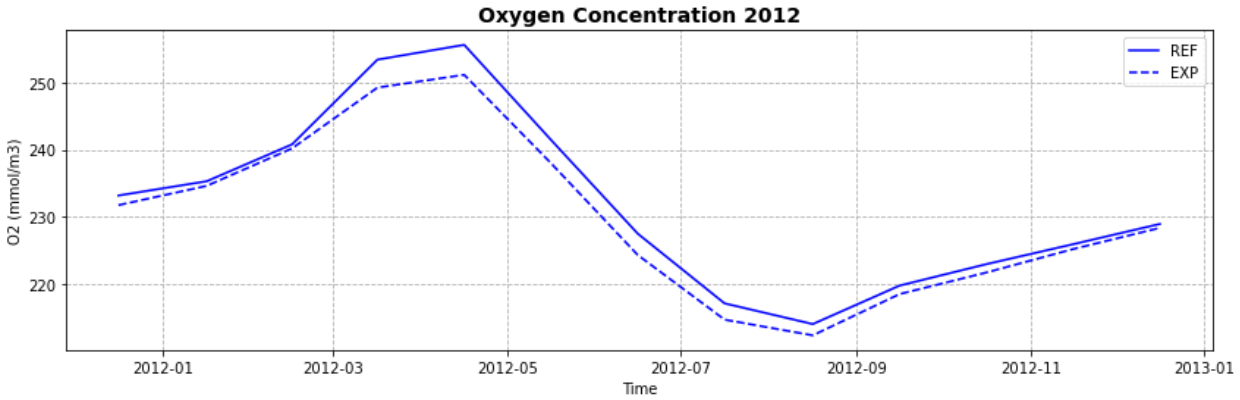

Figure 22: Temporal evolution of mean surface oxygen concentration in 2012 for REF (solid line) and EXP (dashed line) in the North Aegean Sea.

We examine the carbonate system variables data, focusing on alkalinity and Dissolved Inorganic Carbon (DIC) in the NA for the year 2012 by comparing the two experiments (REF and EXP). The mean difference between REF and EXP (REF–EXP) was consistently positive (**Figure 23**), indicating that the BSW inflow enriches the NA with inorganic nutrients. Both alkalinity and DIC anomalies exhibited similar fluctuations between the two experiments throughout the year. The peak anomalies for both alkalinity and DIC occurred in July, with mean surface value of +148.6 mmol/m^3 for alkalinity and +120.8 mmol/m^3 for DIC. Conversely, the

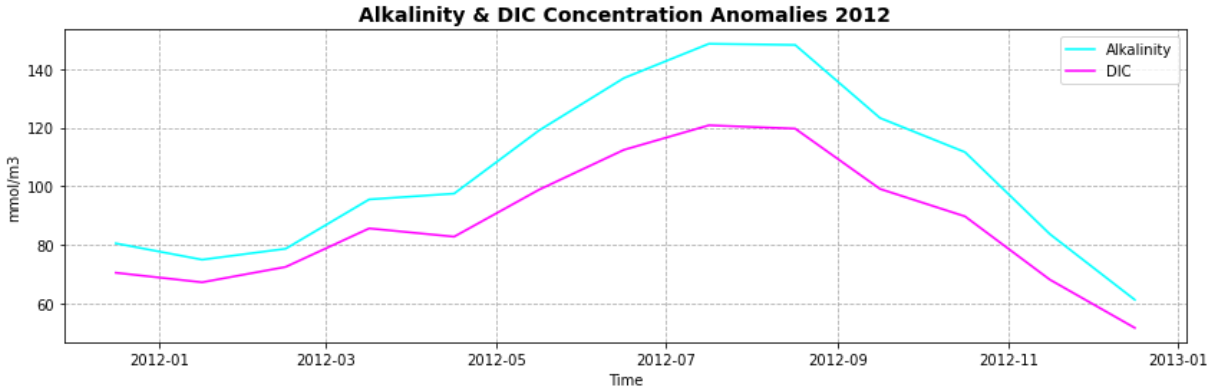

Figure 23: Temporal evolution of mean surface Alkalinity (blue) and Dissolved Inorganic Carbon (magenta) concentration anomalies in 2012 in the North Aegean Sea.

lowest (positive) anomalies were observed in December, measuring +61.3 mmol/m^3 for alkalinity and +51.8 mmol/m^3 for DIC. The reason for the peak values in July can be attributed to the heightened inflow of BSW into the NA during the summer months, which reaches its maximum during this period. Consequently, the absence of BSW inflow during this time leads to the highest anomaly values for alkalinity and DIC. This result provides insight into the seasonal variations of carbonate system variables in the NA and highlights the significant influence of BSW on these fluctuations.

Figure 24 displays the mean surface anomalies of inorganic nutrients, with particular focus on the evolution of silicate, nitrate, and phosphate levels throughout the year. The silicate anomaly exhibits the most intriguing pattern, peaking at +1.23 mmol/m^3 in February and reaching its highest decreasing value of -0.44 mmol/m^3 in July. Similarly, nitrate attains its highest anomaly value of +0.9 mmol/m^3 in February, while in August, it reaches the maximum decrease of -0.1 mmol/m^3. In contrast, phosphate anomalies remain consistently positive but relatively low over the entire year, with a peak increase of +0.17 mmol/m^3 in March and a minimum increase of +0.07 mmol/m^3 in December. Both silicate and nitrate anomalies show a similar pattern of increment from January to February and reduction from March to August. From the temporal evolution of inorganic nutrients anomalies, it is evident that BSW inflow contributes to the increase of phosphate levels throughout the year. Regarding silicate and nitrate, BSW plays a significant role in raising its concentration from December to mid-February.

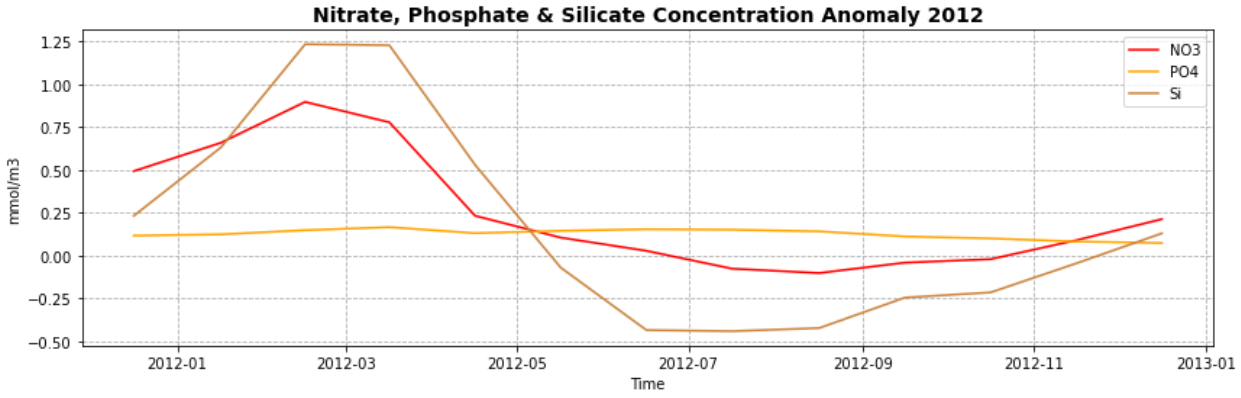

Figure 24: Temporal evolution of mean surface nitrate (red), phosphate (orange) and silicate (brown) concentration anomalies in 2012 in the North Aegean Sea.

3.4.3 Mean annual average vertical profiles

Moving forward, we present the mean annual average profiles of the biogeochemical variables, which were previously investigated for the North Aegean Sea.

Figure 25 illustrates the regional mean chlorophyll concentration vertical profile within the depth of 0-220 m for each experiment. Notably, the mean chlorophyll levels within the first ~70 m are higher in the REF (solid line) compared to the EXP (dashed line). Both experiments exhibit their peak concentrations at the surface (0.43 gChl/m^3 in REF and 0.31 gChl/m^3 in EXP). Moreover, we observe an annual subsurface chlorophyll peak consistently occurring at a depth of around 11.41 m in both experiments, which registers a value of 0.40 gChl/m^3 in REF, contrasting with the 0.30 gChl/m^3 observed in EXP.

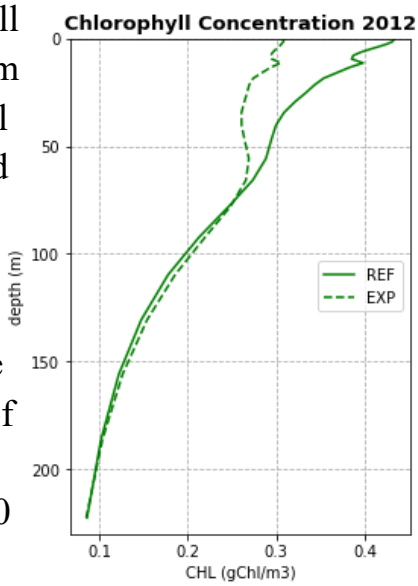

***Figure 25**: Mean annual average vertical profile of chlorophyll concentration of the NA in 2012 along the zonal direction.*

Likewise, **Figure 26** depicts the regional mean oxygen concentration vertical profile. It's noteworthy that oxygen levels within the initial ~45 m are greater in the REF (solid line) compared to the EXP (dashed line). In the REF, the peak oxygen value is observed at 40.34 m, measuring 237.15 mmol/m^3, whereas in the EXP, it appears at a deeper point, around 47.37 m, and nearly matches the REF's maximum value, reaching approximately 237.23 mmol/m^3. Below ~47 m, the oxygen levels in the EXP surpass those in the REF. This can be attributed to the weakening of stratification in EXP scenario, during the initial years of the experiment, facilitating the sinking of dense high-oxygen surface waters (as discussed in subsection 3.3) and thus, significantly increasing the mean annual basin-average oxygen concentration at deeper layers in the EXP scenario.

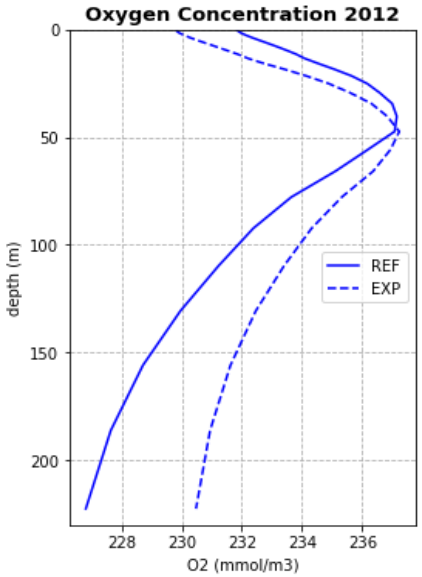

***Figure 26**: Mean annual average vertical profile of oxygen concentration of the NA in 2012 along the zonal direction.*

We now turn our attention to the analysis of key carbonate system variables' vertical profiles, specifically Alkalinity and Dissolved Inorganic Carbon (DIC), within the depth range of 0 to 220 m, as depicted in **Figure 27**. It is evident that across all depths in this range, both Alkalinity and DIC exhibit higher levels in the REF experiment compared to the EXP scenario. Of particular interest is the observation that within REF, DIC attains its peak value of 2492.8 mmol/m^3 at the surface, whereas within the EXP condition, the highest DIC value of 2405.2 mmol/m^3 is recorded at a depth of approximately 220 m. Additionally, it's worth noting that the range of values for both Alkalinity and DIC profiles in the EXP condition is narrower than that observed in the REF condition across the entire 0 – 220-meter depth range.

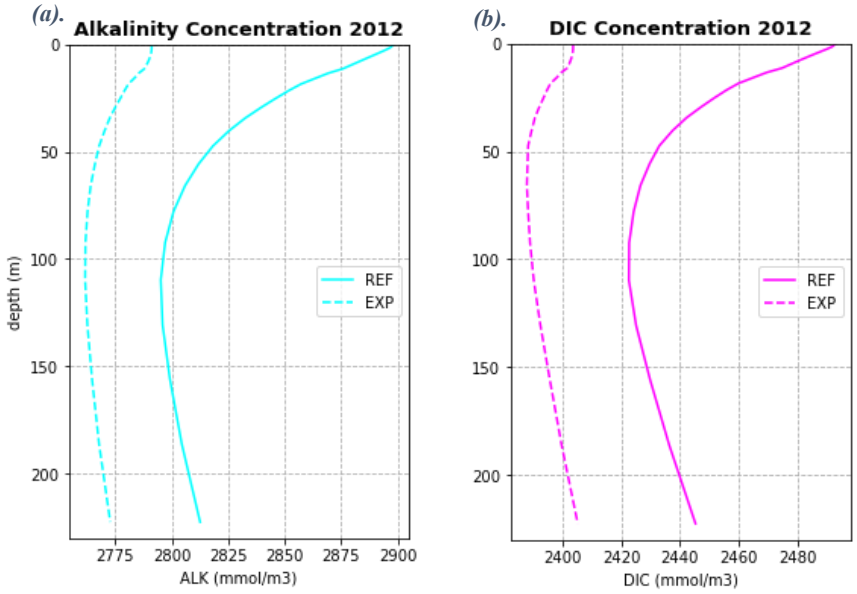

Figure 27: Mean annual average vertical profile of ***(a)*** *Alkalinity and* ***(b)*** *DIC concentration of the North Aegean in 2012. The solid lines refer to the REF case, while the dashed ones correspond to EXP.*

Finally, we investigate the mean annual average vertical profiles of inorganic nutrients, such as phosphate, nitrate, and silicate, as depicted in **Figure 28**. It's worth noting that in both experiments, and for all three variables, their mean values demonstrate a tendency to peak at depths exceeding 200 m. Furthermore, throughout 0 to 200 m, the values observed in the REF experiment consistently surpass those recorded in the EXP scenario. Hence, it can be inferred that BSW plays a critical role in elevating the basin-mean levels of both inorganic nutrients and carbonate variables, not only at the surface, but also throughout various depths.

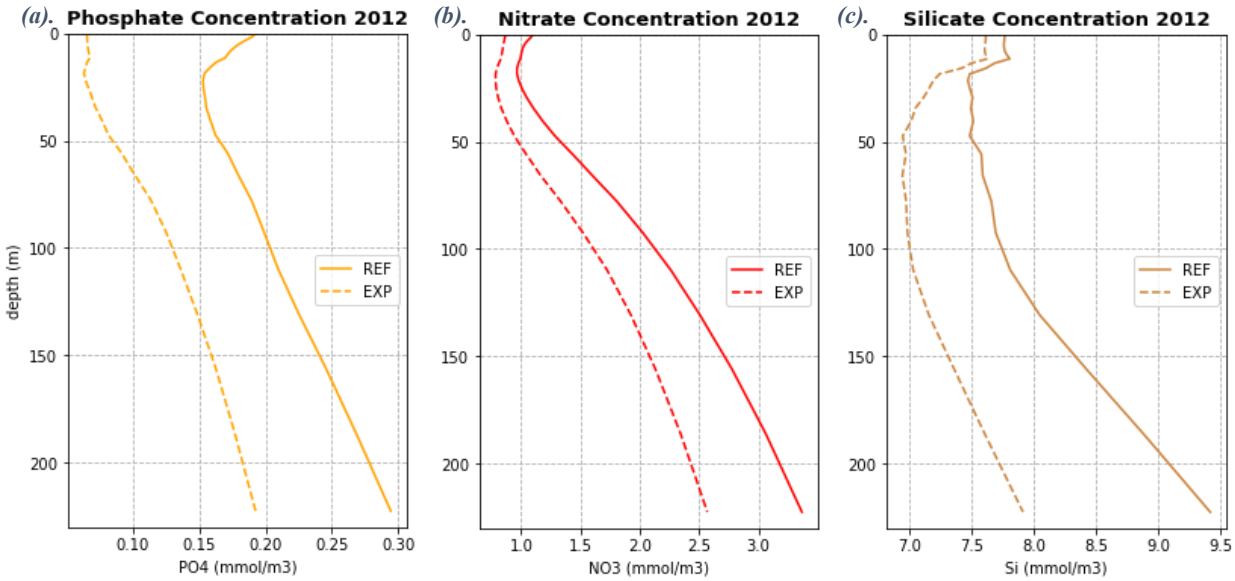

***Figure 28**: Mean annual average vertical profile of **(a).** phosphate, **(b).** nitrate and **(c).** silicate concentration of the North Aegean in 2012 along the zonal direction.*

Chapter 4

Summary and conclusions

This thesis aimed to assess the impact of the BSW inflow on the Aegean dynamics and biogeochemistry, employing a twin numerical model experiment. To achieve this, we utilized a coupled ocean–biogeochemical configuration of the ocean model NEMO at 1/12º resolution for the North Aegean region and for a 5-year timeframe, from 2008 to 2012. In our results we focus on the last year of the study, 2012. We analyze the outcomes of two distinct experiments, both sharing identical experimental setups except for one crucial difference. This difference lies in the fact that the first experiment represents the actual conditions of the study area during the study period, while the second experiment represents a hypothetical scenario where the Dardanelles Strait is sealed off, leading to the complete absence of BSW inflow into the Aegean. The results are primarily focused on the temporal and seasonal spatial variability of upper-ocean and vertical thermohaline and biogeochemical properties for each experiment.

Regarding thermohaline variables, we observed notable differences between the two experiments, primarily in terms of salinity. These differences highlight that the BSW inflow has a substantial impact on reducing salinity levels, not only at the surface (SSS), but also in deeper layers of the North Aegean. Furthermore, the temporal evolution of SSS displayed a nearly identical pattern in both experiments, except for the seasonal peak value, which was obtained in winter, in REF, aligning with what was expected, and in summer in EXP. When examining the seasonal distribution of SST, we noted that BSW exerts a cooling effect during the winter season and creates a warmer plume, compared to the surrounding area, in the summer. However, it's worth noting that BSW did not significantly influence the overall temporal evolution of SST. Additionally, our analysis revealed that BSW serves as a significant contributor to Kinetic Energy, particularly during the summer season. Upon examination of the annual circulation patterns in each experiment, we concluded that BSW inflow enhances the formation of mesoscale eddies in the North Aegean. The

cyclonic formation around Sporades Islands was found significantly intensified by the BSW inflow, potentially leading to enhanced vertical mixing processes in the western part of the basin and thus, facilitating deep water formation during the winter.

To further assess BSW's influence on deep water formation processes of the basin we examined MLD differences between the experiments, in addition to potential density and vertical oxygen levels. Our results indicate that, in the winter season, regions experiencing the most significant changes in thermohaline properties due to the absence of BSW inflow (EXP) coincide with areas where the MLD extends to greater depths in EXP. Furthermore, we noted that when there is no BSW inflow (EXP), there are higher potential density levels and increased oxygen concentrations in depths below 700 m, during the winter season. This suggests that the absence of BSW (EXP) led to the sinking of dense high-oxygen surface waters. We speculate that this phenomenon could be initiated by a weakened salinity gradient, leading to a reduced potential density gradient and consequently, to a weaker stratification and enhanced deep water formation processes. Therefore, we conclude that BSW inflow has the potential to hinder deep water formation processes in the North Aegean, in winter. Moreover, the occurrence of deep water formation in the study area is primarily influenced by changes in the salinity gradient.

Our study highlights the substantial influence of BSW inflow on the North Aegean biogeochemical characteristics, as well. We observed significantly higher chlorophyll levels in the REF experiment, where BSW inflow was present, both in the surface and deeper layers (0-70m). Oxygen concentrations exhibited a contrast between surface and deeper layers: surface oxygen increased with BSW inflow, while deeper layers showed a decrease. Furthermore, the intensified cyclonic formation around Sporades was found to potentially lower average surface oxygen levels in this area during winter.

Carbonate system variables' concentrations, specifically DIC and Alkalinity were also increased when there was BSW inflow into the North Aegean. The seasonality of the BSW inflow, with peak rates occurring in summer (Tzali et al., 2010), significantly influenced DIC and Alkalinity concentrations, with their values peaking during the summer season. Finally, we assessed the impact of BSW inflow on various inorganic nutrients such as phosphate, nitrate, and silicate. We observed

that BSW played a crucial role in elevating phosphate levels throughout the year. Additionally, surface nitrate and silicate levels increased due to BSW inflow during winter and spring but decreased during summer and autumn. Upon examination of the mean annual average vertical profiles, we found that BSW significantly raises the DIC and Alkalinity concentrations, as well as inorganic nutrients' (phosphate, nitrate, silicate) concentrations throughout the 0-220m depth range. In summary, our findings lead us to conclude that BSW inflow enhances nutrient concentrations, thereby boosting the productivity of the North Aegean Sea.

Further study would encompass a more extended simulation period which would enable us to assess how our findings might impact the central and southern Aegean regions, as well as the broader Eastern Mediterranean Sea. Given the ongoing trend of rising salinity levels in the Mediterranean, this extended study could potentially provide valuable insights into forecasting future alternations on thermohaline characteristics and circulation patterns within the region.

Bibliography

- Androulidakis YS, Krestenitis Y, Kourafalou VH. (2012b). Connectivity of North Aegean circulation to the Black Sea water budget. *Continental Shelf Research*, 48: 8-26. DOI: https://doi.org/10.1016/j.csr.2012.08.019

- Aumont O, Ethé C, Tagliabue A, Bopp L, and Gehlen M. (2015). PISCES-v2: an ocean biogeochemical model for carbon and ecosystem studies. *Geoscientific Model Development*, 8(8):2465–2513. DOI: 10.5194/gmd-8-2465-2015. URL: https://www.geosci-model-dev.net/8/2465/2015/

- Barbieux M, Uitz J, Bricaud A, Organelli E, Poteau A, Schmechtig C, Gentili B, Obolensky G, Leymarie E, Penkerc'h C, D'Ortenzio F. (2018). Assessing the variability in the relationship between the particulate backscattering coefficient and the Chlorophyll a concentration from a global biogeochemical-Argo database. *J. Geophys. Res. Oceans.,* 123:1229–1250. DOI: https://doi.org/10.1002/2017JC013030

- Beşiktepe ŞT, Sur Hİ, Özsoy E, Latif MA, Oguz T, Ünlüata Ü. (1994). The circulation and hydrography of the Marmara Sea. *Prog. Oceanogr.,* 34:285–334. DOI: 10.1016/0079-6611(94)90018-3

- De Madron XD, Guieu C, Sempere R, Conan P, Cossa D, D'Ortenzio F, Estournel C, Gazeau F, Rabouille C, Stemmann L, Bonnet S, et al. (2011). Marine ecosystems' responses to climatic and anthropogenic forcings in the Mediterranean. *Prog. Oceanogr.,* 91:97–166. DOI: https://doi.org/10.1016/j.pocean.2011.02.003

- D'Ortenzio F, D'Alcalà MR. (2009). On the trophic regimes of the Mediterranean Sea: a satellite analysis. *Biogeosciences,* 6:139–148. DOI: https://doi.org/10.5194/bg-6-139-2009

- Gertman I, Pinardi N, Popov Y, Hecht A. (2006). Aegean Sea water masses during the early stages of the Eastern Mediterranean Climatic Transient (1988–1990). *J. Phys. Oceanogr.,* 36(9):1841–1859. DOI: https://doi.org/10.1175/JPO2940.1

- GRDC. (2014). Global Freshwater Fluxes Into the World Oceans / Online Provided By Global Runoff Data Centre, two thousand fourteenth ed. Federal Institute of Hydrology (BfG), Koblenz, URL: https://www.bafg.de/GRDC/EN/02_srvcs/24_rprtsrs/report_44.pdf?__blob=publicationFile, accessed 10 2020.

- Griffies SM, Harrison MJ, Pacanowski RC, Rosati A. (2004). A Technical Guide to MOM4, GFDL Ocean Group Technical Report No. 5. NOAA/Geophysical Fluid Dynamics Laboratory. Version prepared on August 23, 2004. URL: www.gfdl.noaa.gov

- Hersbach H, Bell B, Berrisford P, Biavati G, Horányi A, Muñoz Sabater J, Nicolas J, Peubey C, Radu R, Rozum I, Schepers D, Simmons A, Soci C, Dee D, Thépaut J N. (2023) ERA5 hourly data on single levels from 1940 to present, *Copernicus Climate Change Service (C3S) Climate Data Store (CDS)* [data set]. DOI: 10.24381/cds.adbb2d47

- Ignatiades L, Psarra S, Zervakis V, Pagou K, Souvermezoglou E, Assimakpoulou G, Gotsis-Skretas O. (2002). Phytoplankton size-based dynamics in the Aegean Sea (Eastern Mediterranean). *J. Mar. Syst.,* 3:11–28. DOI: 10.1016/S0924-7963(02)00132-X

- Jarosz E, Teague WJ, Book JW, Beşiktepe ŞT. (2012). Observations on the characteristics of the exchange flow in the Dardanelles Strait. *J. Geophys. Res.,* 117:C11012. DOI:10.1029/2012JC008348

- Kalaroni S, Tsiaras K, Petihakis G, Economou-Amilli A, Triantafyllou G. (2020). Modelling the Mediterranean pelagic ecosystem using the POSEIDON ecological model. Part I: Nutrients and chlorophyll-a dynamics. *Deep Sea Research Part II*, 171. DOI: https://doi.org/10.1016/j.dsr2.2019.104647

- Kalaroni S, Tsiaras K, Petihakis G, Economou-Amilli A, Triantafyllou G. (2020). Modelling the Mediterranean pelagic ecosystem using the POSEIDON ecological model. Part II: Biological dynamics. *Deep-Sea Research Part II*, 171 DOI: https://doi.org/10.1016/j.dsr2.2019.104711

- Karagiorgos J, Vervatis V, Sofianos S. (2023). The effect of water turbidity on the upper-ocean properties and dynamics in the Mediterranean and Black Seas, *EGU General Assembly 2023,* Vienna, Austria, 24–28 Apr 2023, EGU23-3520. DOI: https://doi.org/10.5194/egusphere-egu23-3520

- Kourafalou VH, Barbopoulos K. (2003). High resolution simulations on the North Aegean Sea seasonal circulation. *Ann. Geophys,* 21:251–265. DOI: 10.5194/angeo-21-251-2003

- Krom MD, Kress N, Brenner S, Gordon LI. (1991). Phosphorus limitation of primary productivity in the eastern Mediterranean Sea. *Limnol. Oceanogr.,* 36:424–432. DOI: https://doi.org/10.4319/lo.1991.36.3.0424

- Krom MD, Emeis KC, Van Cappellen P. (2010). Why is the Eastern Mediterranean phosphorus limited? *Prog. Oceanogr.*, 85:236–244. DOI: https://doi.org/10.1016/j.pocean.2010.03.003

- Lavigne H, D'Ortenzio F, D'Alcalà MR, Claustre H, Sauzède R, Gacic M. (2015). On the vertical distribution of the chlorophyll a concentration in the Mediterranean Sea: a basin-scale and seasonal approach. *Biogeosciences,* 12:5021–5039. DOI: 10.5194/bg-12-5021-2015

- Lykousis V, Chronis G, Tselepidis A, Price NB, Theocharis A, Siokou-Frangou I, Van Wambeke F, Danovaro R, Stavrakakis S, Duineveld G, Georgopoulos D, Ignatiades L, Souvermezoglou A, Voutsinou-Taliadouri F. (2002). Major outputs of the recent multidisciplinary biogeochemical researches undertaken in the Aegean Sea. *J. Mar. Syst.,* 33–34:313–334. DOI: https://doi.org/10.1016/S0924-7963(02)00064-7

- Mayorga E, Seitzinger SP, Harrison JA, Dumont E, Beusen AHW, Bowman AF, Fekete BM, Kroeze C, Van Drecht G. (2010). Global Nutrient Export from WaterSheds 2 (NEWS 2): model development and implementation, *J. Environ. Modell. Softw.,* 25:837–853. DOI: https://doi.org/10.1016/j.envsoft.2010.01.007

- Madec G. and the NEMO System Team. (2023). NEMO Ocean Engine Reference Manual, *Zenodo*. DOI: https://doi.org/10.5281/zenodo.8167700

- Mavropoulou AM, Mantziafou A, Jarosz E, Sofianos S. (2016). The influence of Black Sea Water inflow and its synoptic time-scale variability in the North Aegean Sea hydrodynamics. *Ocean. Dyn.*, 66:195–206. DOI: 10.1007/s10236-016-0923-5

- Oğuz T, Sur IH. (1989). A 2-layer model of water exchange through the Dardanelles strait. *Oceanol. Acta.,* 12(1):23–31. URL: https://archimer.ifremer.fr/doc/00106/21750/

- Petihakis G, Tsiaras K, Triantafyllou G, Kalaroni S, Pollani A. (2014). Sensitivity of the N. Aegean sea ecosystem to black sea water inputs. *Mediterr. Mar. Sci.,* 790–804. DOI: 10.12681/MMS.955

- Polat C, Tugrul S. (1996). Chemical exchange between the mediterranean and black sea via the Turkish straits. *CIESM science series. Bull. Inst. Oceanogr*., 2 (17):167–186. URL: http://old.ims.metu.edu.tr/pdf/1861.pdf

- Roether W, Manca B, Klein B, Bregant D, Georgopoulos D, Beitzel V, Kovacevic V, Luchetta A. (1996). Recent changes in the Eastern Mediterranean deep waters. *Science*, 271:333-335. DOI: 10.1126/science.271.5247.333

- Siokou-Frangou I, Bianchi M, Christaki U, Christou ED, Giannakourou A, Gotsis O, Ignatiades L, Pagou K, Pitta P, Psarra S, Souvermezoglou E. (2002). Carbon flow in the planktonic food web along a gradient of oligotrophy in the Aegean Sea (Mediterranean Sea). *J. Mar. Syst.,* 33:335–353. DOI: https://doi.org/ 10.1016/S0924-7963(02)00065-9

- Siokou-Frangou I, Zervoudaki S, Christou E, Zervakis V, Georgopoulos D. (2009). Variability of mesozooplankton spatial distribution in the North Aegean Sea, as influenced by the Black Sea waters outflow. *J. Mar. Syst.,* 78:557–575. DOI: 10.1016/J.JMARSYS.2008.12.025

- Siokou-Frangou I, Christaki U, Mazzocchi MG, Montresor M, Ribera d'Alcalà M, Vaqué D, Zingone A. (2010). Plankton in the open Mediterranean Sea: a review. *Biogeosciences*, 7:1543–1586. DOI: https://doi.org/10.5194/bg-7-1543-2010

- Sofianos S, Skliris N, Vervatis V, Olson D, Kourafalou V, Laskaratos A, Johns W. (2005). On the forcing mechanisms of the Aegean Sea surface circulation. *Geophys. Res. Abst.,* 7:04223.

- SoHelME. (2005). *State of the Hellenic marine environment*. HCMR

- Takahashi T, Sutherland SC, Chipman DW, Goddard JG, Newberger T, Sweeney C. (2014). Climatological Distributions of pH, pCO2, Total CO2, Alkalinity, and CaCO3 Saturation in the Global Surface Ocean. ORNL/CDIAC-160, NDP-094. Carbon Dioxide Information Analysis Center,

Oak Ridge National Laboratory, U.S. Department of Energy, Oak Ridge, Tennessee. DOI: 10.3334/CDIAC/OTG.NDP094]

- Theocharis A, Nittis K, Kontoyannis H, Papageorgiou E, Balopoulos E. (1999). Climatic changes in the deep waters of the Aegean sea and their influence in the deep thermohaline circulation of the Eastern Mediterranean (1986–1997). *Geophysical Research Letters*, 20:1617–1620. DOI: 10.1029/1999GL900320

- Thingstad FT, Krom MD, Mantoura RFC, Flaten G, Groom S, Herut B, Kress N, Law CS, Pasternak A, Pitta P, Psarra S, Rassoulzadegan F, Tanaka T, Tselepides A, Wassmann P, Woodward EMS, Wexels-Riser C, Zodiatis G, Zohary T. (2005). Nature of phosphorus limitation in the ultraoligotrophic Eastern Mediterranean. *Science*, 309:1068–1071. DOI: 10.1126/science.1112632

- Tragou E, Petalas S, Mamoutos I. (2022) Air-Sea Interaction - Heat and freshwater fluxes in the Aegean Sea. (2022). *The Aegean Sea Environment: The Natural System*; *Barcelo D, Kostianoy AG, Eds.; The Handbook of Environmental Chemistry*, Chapter A-10. DOI: 10.1007/698_2021_841

- Turley CM, Bianchi M, Christaki U, Conan P, Harris JRW, Psarra S, Ruddy G, Stutt ED, Tselepides A, Van Wambeke F. (2000). Relationship between primary producers and bacteria in an oligotrophic sea - the Mediterranean and biogeochemical implications. *Mar. Ecol. Prog. Ser.*, 193:11–18. DOI: https://doi.org/10.3354/meps193011

- Tzali M, Sofianos S, Mantziafou A, Skliris N. (2010). Modelling the impact of Black Sea water inflow on the North Aegean Sea hydrodynamics. *Ocean. Dyn.,* 60:585–596. DOI: 10.1007/s10236-010-0277-3

- Ünlüata U, Oğuz T, Latif MA, Oszoy E. (1990). On the physical oceanography of Turkish Straits. *Pratt LJ (ed) The physical oceanography of sea straits*. Kluwer, Netherlands, 25–60. DOI: 10.1007/978-94-009-0677-8_2

- Varlas G, Vervatis V, Spyrou C, Papadopoulou E, Papadopoulos A, Katsafados P. (2020). Investigating the impact of atmosphere–wave–ocean interactions on a Mediterranean tropical-like cyclone. *Ocean Modelling,* 153:101675. DOI: https://doi.org/10.1016/j.ocemod.2020.101675

- Vervatis V, Sofianos S, Skliris N, Somot S, Lascaratos A, Rixen M. (2013). Mechanisms controlling the thermohaline circulation pattern variability in the Aegean-Levantine region. A hindcast simulation (1960-2000) with an eddy resolving model. *Deep-Sea Res. Part I*, 74:82-97. DOI: https://doi.org/10.1016/j.dsr.2012.12.011

- Vlasenko VI, Stashchuk NM, Ivanov VA, Nikolaenko EG, Uslu O, Benli H. (1996). Influence of the water exchange through the Dardanelles on the thermohaline structure of the Aegean Sea. *Bulletin de I'Institut oceanographique 17, CIESM Science Series no. 2*. URL: https://ciesm.org/online/monographs/CSS-2/CSS_2_147_165.pdf

- Zervakis V, Georgopoulos D, (2002), Hydrology and circulation in the North Aegean (eastern Mediterranean) throughout 1997 and 1998. *Mediterr. Mar. Sci.,* 3:5–19. DOI: 10.12681/mms.254

- Zervakis V, Georgopoulos D, Drakopoulos PG. (2000). The role of the North Aegean Sea in triggering the recent Eastern Mediterranean climatic changes. *J. Geophys. Res.,* 105(C11):26103–26116. DOI: https://doi.org/10.1029/2000JC900131

- Zodiatis G. (1994). Advection of the Black Sea water in the North Aegean Sea. *Glob. Atmos. Ocean Syst.,* 2:41–60.

Acknowledgements

I would like to acknowledge my supervisor, Sarantis Sofianos, for giving me the opportunity to work on such an interesting subject and for cultivating a great interest for the field of Physical Oceanography within me throughout these study years. Many thanks to Ioannis Karagiorgos for his valuable and crucial contribution throughout the implementation of this thesis and to Dr. Vassilios Vervatis for his helpful insights and suggestions. Our cooperation was of foremost importance for this project. Last but not least, I want to thank my family and friends for their continued support and encouragement during my studies.

This work was supported by computational time granted from the National Infrastructures for Research and Technology S.A. (GRNET S.A.) in the National HPC facility - ARIS - under project pr013013 (BOFCOAM). The development of the numerical models was also supported by the Hellenic Foundation for Research and Innovation (HFRI) under the 4th Call for HFRI PhD Fellowships (Fellowship Number: 10793).